ARMY RESEARCH LABORATORY

Nondestructive Evaluation of a Metal Matrix Composite

by William S. de Rosset

ARL-TR-3118 **December 2003**

NOTICES

Disclaimers

The findings in this report are not to be construed as an official Department of the Army position unless so designated by other authorized documents.

Citation of manufacturer's or trade names does not constitute an official endorsement or approval of the use thereof.

Destroy this report when it is no longer needed. Do not return it to the originator.

Army Research Laboratory
Aberdeen Proving Ground, MD 21005-5069

ARL-TR-3118 **December 2003**

Nondestructive Evaluation of a Metal Matrix Composite

William S. de Rosset
Weapons and Materials Research Directorate, ARL

REPORT DOCUMENTATION PAGE	Form Approved OMB No. 0704-0188

1. REPORT DATE *(DD-MM-YYYY)*	2. REPORT TYPE	3. DATES COVERED (From - To)
December 2003	Final	1 October 2002–30 September 2003

4. TITLE AND SUBTITLE	5a. CONTRACT NUMBER
Nondestructive Evaluation of a Metal Matrix Composite	5b. GRANT NUMBER
	5c. PROGRAM ELEMENT NUMBER

6. AUTHOR(S)	5d. PROJECT NUMBER
William S. de Rosset	AH 84
	5e. TASK NUMBER
	5f. WORK UNIT NUMBER

7. PERFORMING ORGANIZATION NAME(S) AND ADDRESS(ES)	8. PERFORMING ORGANIZATION REPORT NUMBER
U.S. Army Research Laboratory ATTN: AMSRD-ARL-WM-MD Aberdeen Proving Ground, MD 21005-5069	ARL-TR-3118

9. SPONSORING/MONITORING AGENCY NAME(S) AND ADDRESS(ES)	10. SPONSOR/MONITOR'S ACRONYM(S)
	11. SPONSOR/MONITOR'S REPORT NUMBER(S)

12. DISTRIBUTION/AVAILABILITY STATEMENT

Approved for public release; distribution is unlimited.

13. SUPPLEMENTARY NOTES

14. ABSTRACT

Samples of aluminum metal matrix composites (AlMMCs) have been examined with nondestructive evaluation techniques. A literature search identified ultrasonic C-scans as one of the most promising techniques, and this approach was used along with an eddy-current based approach, Meandering Winding Magnetometer (MWM), that also had some potential usefulness for flaw detection. Samples with known flaws were first investigated to ascertain the sensitivity of the equipment. Subsequent tests were performed on samples obtained from the University of Delaware. The findings were that both ultrasonics and MWM could detect gross flaws (cracks, delaminations, lack of matrix infusion, etc.) but that more subtle defects such as fiber waviness could not be detected unequivocally. Since fiber volume content determines to a large extent the strength of the AlMMC, a quantitative relationship between fiber volume content and the sonic velocity was developed. It was also noted that as fiber volume content increased, the ultrasonic signal attenuation increased. High signal attenuation due to high fiber volume content in some of the earlier ultrasonic scans led to a misinterpretation of those scans that was subsequently corrected.

15. SUBJECT TERMS

aluminum metal matrix composites, Nextel 610 fibers, ultrasonic attenuation, nondestructive evaluation, nondestructive testing, Meandering Winding Magnetometer, flaw detection, fiber volume content, delamination

16. SECURITY CLASSIFICATION OF:			17. LIMITATION OF ABSTRACT	18. NUMBER OF PAGES	19a. NAME OF RESPONSIBLE PERSON
a. REPORT	b. ABSTRACT	c. THIS PAGE			William S. de Rosset
UNCLASSIFIED	UNCLASSIFIED	UNCLASSIFIED	UL	46	19b. TELEPHONE NUMBER (*Include area code*) 410-306-0816

Standard Form 298 (Rev. 8/98)
Prescribed by ANSI Std. Z39.18

Contents

List of Figures

List of Tables

Acknowledgments

The author gratefully recognizes the contributions of the following individuals. Thanks go to Jim Burnett of Triton Systems for the sample used in relating fiber volume to sonic velocity. Brad Klotz is acknowledged for making the density measurements on the aluminum metal matrix composite (AlMMC) cylinders and parts. Kyu Cho is recognized for assisting in taking pictures of the experimental apparatus. Jim Campbell and Scott Grendahl took the micrographs of the AlMMC samples. Robert Lyons of Jentek Sensors provided the instruction and technical support for making the Meandering Winding Magnetometer (MWM) measurements. Andy Washabaugh of Jentek Sensors provided the technical background and careful editing of the text dealing with MWM theory. Many helpful technical discussions on metal matrix composites were conducted with Ian Hall (University of Delaware) and Travis Bogetti. Ian Hall provided the flat plate samples examined in section 6 of this report. Mike Fick of 3M Corporation is thanked for providing samples with known flaws. Marc Pepi (former U.S. Army Research Laboratory employee and now at the Naval Surface Weapons Center, China Lake, CA) helped with the literature search. Finally, thanks go to Chris Hoppel for his support and encouragement of this work.

1. Introduction

The U.S. Army's need for high-strength, light-weight materials is responsible for current research and development efforts in the area of metal matrix composites. In particular, the U.S. Army Research Laboratory (ARL) has been investigating the use of continuous alumina fibers (Nextel 610*) in an aluminum (A1) or A1 alloy matrix (Bender et al., report in progress; Hoppel et al., 2000, 2002). This material has exhibited very high compressive strength and very good high-temperature properties (as compared to traditional organic fiber matrix materials). Two applications currently being pursued are a metal matrix artillery shell and a composite gun tube (steel liner with a metal matrix overwrap).

The aluminum metal matrix composite (AlMMC) under consideration has traditionally been made with a pressure-cast process where the molten metal is infiltrated into a fiber preform, solidified, and extracted from the mold. More recently, attempts have been made to squeeze-cast the material by injecting the molten metal at high pressure into a mold filled with fiber preform. Finally, AlMMC tape has been produced with the idea of using standard prepreg technology to wrap the tape over a mandrel of the desired geometry and use braze to join the tape layers together.

Each of these manufacturing processes has its own inherent difficulties for producing material that is defect-free. Consequently, there is a need to develop a reliable, quick, and inexpensive method to ensure that the materials produced by any of these processes do not contain defects that would be detrimental to use in their intended applications. For this reason, a survey of current nondestructive evaluation (NDE) techniques was undertaken to determine what approaches might be best to use for quality control of the AlMMC material. The goal was to identify one or more NDE techniques that could be used in a factory setting to ascertain the quality of material produced. (NDE used for health monitoring was not considered here.) This survey is presented in section 2 along with background material on flaws and flaw detection as they might apply to AlMMC.

Section 3 contains a description of material obtained from 3M Corporation that was known to contain defects. These samples were used to help determine the sensitivity of the two NDE techniques chosen for this study.

The literature search led to the conclusion that ultrasonic testing (UT) was a leading candidate for screening this material. However, a new technique called Meandering Winding Magnetometer† (MWM) was also found to have potential. The MWM technique extends eddy

* Nextel 610 is a registered trademark of the 3M Corporation.

† Meandering Winding Magnetometer is a registered trademark of JENTEK Sensors, Inc.

current technology by measuring absolute values of conductivity and lift-off. These techniques will be described in sections 4 and 5. Each of these sections will present measurements made on samples with known defects to indicate the ability of each technique to locate flaws.

AlMMC plates made by 3M Corporation and provided to ARL by the University of Delaware were examined with both UT and MWM. While most of these plates appeared to be defect-free, a few had ultrasonic C-scans that indicated the existence of possible flaws. These plates were sectioned to correlate the microstructure with the ultrasonic observations. The results of the ultrasonic measurements on these plates as well as a representative micrograph of the interior of a sample are presented in section 6.

Section 7 contains a discussion of the results and the relative merits of both NDE approaches. Section 8 summarizes the findings of this investigation.

2. Literature Survey

While metal matrix composites (MMCs) have been in existence for over 40 years, they did not come into widespread use until a low-cost source of fibers was developed in the mid-80s (Chin, 2002). This literature survey covers a time span reaching from 1970 to the present. However, most of the reports uncovered in this search are from the 1990s. The following keywords used for this search are given in table 1.

Table 1. Keywords for literature search.

NDE of fiber-reinforced materials
NDE of fiber-reinforced MMCs
NDE of fiber-reinforced metals
NDE of cylinders
NDT of AlMMCs
Alumina fiber-reinforced Al + ultrasonics
Alumina-A1 composites + UT

The survey has shown that ultrasonic techniques have been the most common means for examining MMCs. Computed tomography and thermography have also been used to some extent. To a much lesser extent neutron diffraction and eddy current measurements have been used.

One of the earlier papers written on this subject was an exhaustive study of the sensitivity of flaws to NDE techniques by Schramm and Daniel (1982). They purposely introduced known flaws into an MMC made of alumina fibers in a magnesium alloy (ZE41A). The types of flaws examined were fiber-matrix debonding, porosity, fiber misalignment, fiber fracture, nonuniform fiber distribution, and matrix fracture. The NDE techniques they used were ultrasonic inspection

(primarily C-scan), ultrasonic attenuation, ultrasonic backscattering, wave propagation velocity, and radiography. The authors presented a summary of their findings in a seven-row, nine-column table. They also made the general statement that C-scans were the most useful type of NDE for MMCs, but that other NDE techniques provided valuable additional information.

A comprehensive review of the state-of-the-art in NDE of MMCs was undertaken by the National Research Council in the early 1980s (Pipes and committee, 1983). A thorough literature search at that time revealed only a limited amount of information in this area. Much of the report was supplemented by the National Materials Advisory board member's own experience.

One obvious technique not mentioned by others is visual inspection. They go on to list possible NDE techniques. They eliminate magnetic methods because constituents of MMCs to that point were nonmagnetic. Other methods, such as scanned acoustic holography, dye penetrant, and synthetic aperture focusing techniques, have not found widespread use since the early 1980s.

Another comprehensive paper found in this survey was by Y. Bar-Cohen (1986) who reviewed NDE techniques used to examine aircraft structures. From a practical point of view, Bar-Cohen concluded that due to the many sources of error (e.g., surface roughness, the coupling system used, internal reflections, etc.) ultrasonics can only detect gross flaws in fiber-reinforced materials. For an ultrasonic wave to detect a flaw, the wave length needs to be on the order (or smaller) of the flaw size itself. If the flaw is the size of a fiber, then the ultrasonic wave with wavelength small enough to detect it would be highly scattered by the large number of fibers contained in the sample. Bar-Cohen lists the types of defects produced in the fabrication of fiber-reinforced composites (generally organic fibers in a plastic matrix). Many of these defects suggest similar types of defects in MMCs as shown in table 2.

Table 2. Possible defects induced during fabrication.

Delamination	Wrong lay-up order
Broken fibers	Porosity and voids
Matrix cracking	Incorrect ratio of matrix to fiber volume
Fiber misalignment	—
Inclusions and contamination	—

Note that flaw detection in materials to be used for aircraft structures is generally more stringent due to flight safety concerns.

Many of these defects have the potential to be detected by ultrasonics if they are large enough. For instance, Bar-Cohen cites the detection of a 1 mm in diameter delamination in a graphite-epoxy laminate using time-of-flight ultrasonic measurements. The location accuracy achieved was ± 0.2 mm in depth. While individual micropores cannot be detected, if the density of them is high enough, then they might be detected through a change in attenuation or modulus with ultrasonics or a variation in density through an x-ray scan.

Knowing the processing technology used to make specific MMCs and the type of defect most likely to occur can help determine what type of NDE approach to take. This is demonstrated in a series of papers written by Matikas and coworkers (Matikas and Karpur, 1993; Krishnamurthy et al., 1995; Matikas et al., 1995). The authors examined the interaction of longitudinal and shear waves with a single silicon carbide fiber embedded in a titanium alloy matrix. The fiber was embedded by placing it between two thin sheets of titanium alloy and applying heat and pressure. In some instances, depending on the processing parameters, incomplete consolidation occurred. The ultrasonic methodology developed by Matikas et al. (1995) was able to determine which processes resulted in complete consolidation. The technique was not intended to work on a sample made of a large number of randomly oriented fibers. Rather, it was used to define the processing parameters most likely to result in complete consolidation. As such, the information might have been found through a destructive test more easily.

Chen et al. (1996) also examined the interface between the matrix and reinforcing element. In this case, the material was zirconia particles in a zinc alloy matrix. The authors used a photothermal microscope to delineate the boundary between the particle and matrix. While the microscope could focus down to a minimum diameter of 7 μm and identify near-surface particles of zirconia, it could not distinguish between the different processing techniques used to prepare the samples.

Ultrasonic C-scans have been used by many groups to identify flaws in MMCs. Besides the early work by Schramm and Daniel (1982) and Johnson (1989) conducted a C-scan investigation of an MMC made of boron fibers in an aluminum matrix. The study indicated that gaps between fibers (0.14 mm in diameter) could be detected with a C-scan. The gaps were produced during the fabrication process. This particular material has the boron fibers aligned and in well-defined layers. There was not much detail given about the parameters associated with the C-scan, other than they were produced with an Automation Industries Model S-80 pulse-echo unit. No quantitative correlation could be made between the detected flaw and material properties such as fatigue endurance limits. Tsangarakis et al. (1985) examined an alumina-aluminum MMC plate with a hole in its center and subjected to tension-tension fatigue tests. Differences between C-scan images before and after the fatigue tests provided a measure of the shape of the fatigue damage near the central hole. Fatigue damage consisted primarily of fiber debonding. Canumalla et al. (1992) used C-scans to investigate squeeze-cast aluminum-alumina silicate samples for manufacturing flaws. In this case, the fiber density was relatively low (10%). The researchers identified an area in the center of the sample that gave high ultrasonic damping. This portion of the sample was sectioned to find a high density of small voids, presumably made during the manufacturing process.

An attempt to determine void content on a more quantitative basis was made by Thompson et al. (1991). The authors studied the frequency dependence of the attenuation and related it to the void density. They found that the void content was proportional to da/df, where a is the attenuation and f is the frequency. The proportionality constant (k) was found to depend on the

void morphology (4 for spheres and 2 for flat voids), so that one needs to know what type of void is present a priori. Schwer et al. (1991) used this technique to measure the void content in a graphite-epoxy filament-wound rocket motor case. They found that the void content fell between 2.6% and 7.2%, depending on whether the voids were flat cylinders or spheres. Acid digestion of the sample later confirmed the void content to be 4.4%. An optical microscope was used to examine the void morphology in an intact sample of material. It was found that there were a great variety of void shapes and sizes. The authors concluded that a great deal more work was needed to be conducted to provide a quantitative measure of the void content in these types of materials.

Besides Schramm and Daniel (1982), several groups have used multiple NDE techniques, combined with microstructural (destructive) observations to correlate NDE data with material defects. Hsu et al. (1994) used ultrasonic C-scan, eddy current, and x-ray radiography measurements to probe an MMC made of a nickel-iron-aluminum matrix and tungsten wires. The wires were in three layers and contained 180 wires per layer. The sample dimension was $27.6 \times 18.5 \times 0.72$ mm. Both the eddy current and C-scan returned images that had similar features. The x-ray scan did not correlate well with the other images. A microstructural examination of the sample indicated that there was no correlation between the NDE results and the small amount of porosity present. However, the eddy current and C-scan data correlated with fiber density averaged over the three layers and taking into account the beam widths of the measuring devices.

Tsangarakis et al. (1985) also used multiple NDE techniques along with a microstructural examination to correlate fatigue damage with NDE results. As mentioned above, C-scans were taken before and after fatigue tests were conducted on an MMC made up of an aluminum-lithium matrix and alumina fibers. The authors also used thermography and a limited x-ray examination of the samples. The x-ray approach revealed fatigue cracks but could not detect the striations due to matrix plastic deformation. Interpretation of the thermal measurements was difficult, but the conclusion was that thermography could be used to identify surface fatigue damage in isolated cases.

In investigations of thermal fatigue damage to an alumina fiber-aluminum matrix composite, Bridge et al. (2001) used ultrasonics to track the changes in modulus of cylindrical and flat-plate specimens as a function of the number of cycles. They produced results that were dependent on the specimen geometry (flat plate or cylinder), type of sound wave (longitudinal or shear), and matrix content (pure aluminum or aluminum-copper alloy). In general, substantial reductions in both strength and modulus occurred after 1000 cycles at 300 ºC (20%–30% for the cylindrical alloy matrix specimens and 20%–65% for the cylindrical pure-aluminum matrix specimens). Further work is being done to correlate microstructual observations with the NDE results.

Buchanan et al. (1997) also used NDE techniques to track damage accumulation in MMCs during mechanical testing. Whereas Bridge et al. (2001) made discreet measurements as a

function of cycle number, Buchanan et al. (1997) made continuous measurements. In their experiments, changes in peak-to-peak amplitude of transmitted ultrasound was found to be a good indicator of impending sample failure.

Computed tomography (CT) has been used over 30 years in the medical field but only in the last decade or so has it been used for NDE of fiber-reinforced composites (see, for instance, early work by Ostman and Persson [1988]). The equipment needed to produce CT images of complex parts requires a large capital investment as well as an operator skilled in producing and interpreting the images (Green, 2002). However, CT has the advantage over ultrasonic techniques in that it is not affected as much by surfaces. One example of its use was to examine an MMC made up of silicon carbide fibers in a titanium alloy matrix (Yancey and Baaklini, 1994). The MMC was in the form of a ring and was contained inside a titanium sleeve. The CT scan was able to distinguish density differences within the MMC as well as misalignment between the inner core of MMC and the titanium surround. Microstructural analysis identified fiber packing density variations as the source of the density variations.

Kupperman et al. (1990) used neutron diffraction to measure the strains in an MMC made of silicon carbide fibers in a titanium matrix. (The fibers were aligned parallel to each other.) Because neutrons can penetrate more deeply than x-rays, this approach offers the potential to provide bulk measurements. The internal strains were produced as a result of the difference in coefficients of thermal expansion between the titanium and the silicon carbide and the fact that the composite was made by infiltrating molten titanium into the fibers and then solidifying the composite. The authors measured strains of 0.25% parallel to the fiber direction, which translates into a residual longitudinal stress of 1300 MPa. However, the authors cautioned that there was some uncertainty in the measurements due to fact that the crystal structure of the fibers and the texture of the matrix were not clearly defined.

Numerous papers have been written on using NDE techniques (primarily ultrasonics) to characterize the elastic properties of MMCs. Wu and Ho (1990) used ultrasonic wave time-of-flight measurements to determine the elastic constants of a unidirectional carbon fiber-reinforced composite. Similar work was done by Chien et al. (1994) to investigate the anisotropic nature of MMCs (primarily fiberglass). Canumalla et al. (1994) attempted to measure the Young's modulus of alumina-silicate fibers using an acoustic microscope. Because the fibers were too small for this approach to be useful, the authors measured the Young's modulus on large globular samples of the fiber material (also formed at the same time the fibers are produced). They found that the measurements underpredicted the Young's modulus of the fibers (determined through other means). Dunn and Ledbetter (1995) used ultrasonics to determine the fiber orientation distribution function (a measure of anisotropy) in both silicon carbide-aluminum and alumina-aluminum MMCs. Lee and Park (1995) characterized a squeeze-cast alumina-aluminum MMC in terms of its elastic constants. They also found that the volume fraction of fibers was correlated with the ultrasonic wave velocity. Honarvar and Sinclair (1998) used resonance acoustic spectroscopy to determine the elastic constants of a cylinder made of

Nextel 610 ceramic fibers in an aluminum matrix. The theoretical and measured elastic constants were in good agreement.

Some general conclusions based on the literature survey are summarized below. In this search, emphasis was placed on continuous fibers embedded in a metal matrix. This restriction narrowed the search considerably. While some reports may have been missed, the following conclusions are representative of the state of the art with regard to this specific area:

1. MMCs are inherently difficult to examine with NDE techniques because of their anisotropy and inhomogeneity.
2. Individual microscopic defects in MMCs are extremely difficult to detect with standard NDE techniques; success has been demonstrated in identifying sample-wide defects such as excessive porosity, gross delaminations, variations in fiber density, and fatigue damage.
3. Understanding what the most likely type of material defect in a given MMC is will suggest the NDE approach to take and where to look for the defect. The presence of two types of defects (e.g., porosity and delamination) complicates the NDE evaluation considerably.
4. Defect detection is qualitative in nature; unless some NDE standard is first developed, there is no hope to quantify defect levels. If an NDE standard is used, high dimensional tolerances are required.
5. The ultrasonic C-scan is the most common NDE technique used for probing MMCs. Commercial equipment is readily available to perform attenuation, time-of-flight, and pulse-echo measurements.
6. Ultrasonics is a useful tool for determining the elastic constants of MMCs.
7. Operators skilled in producing and interpreting NDE data are required for meaningful results.

3. Samples With Known Flaws

Five samples of AlMMC were purchased from 3M Corporation. The samples were produced in early attempts to squeeze cast AlMMC material. 3M Corporation had determined that the samples had flaws in them and provided information to ARL as to what types of flaws were present in each sample. Table 3 gives the specifics for these samples.

Sample 121202-1-1 was not machined and did not have smooth surfaces. Consequently, no C-scans were made with this sample. Sample 112202-1-2 was machined and had a small amount of surface roughness where there was incomplete infiltration. Sample 110101-2-1 was listed as

Table 3. 3M sample inventory.

Plate ID	Dimensions (in)	Weight (g)	Defect
112202-1-2	0.12 × 5.91 × 5.94	231.66	Uninfiltrated
121202-1-1	0.187 × 6.1 × 6.1	336.56	Uninfiltrated
6243-1	0.20 × 0 × 2.75 × 6.1	182.43	Copper intermetallic
110102-2-1	0.25 × 1 × 7.125	102.29	Carbon residue
121202-3-2	0.485 × 1.75 × 6.1	282.48	Fiber waviness

having carbon residue. The residue was left over after burning off the epoxy used to manufacture the fiber prepreg. The wave in sample 121202-3-2 was close to the end of thesample and consequently difficult to examine with ultrasonics. This wave is shown in figure 1.

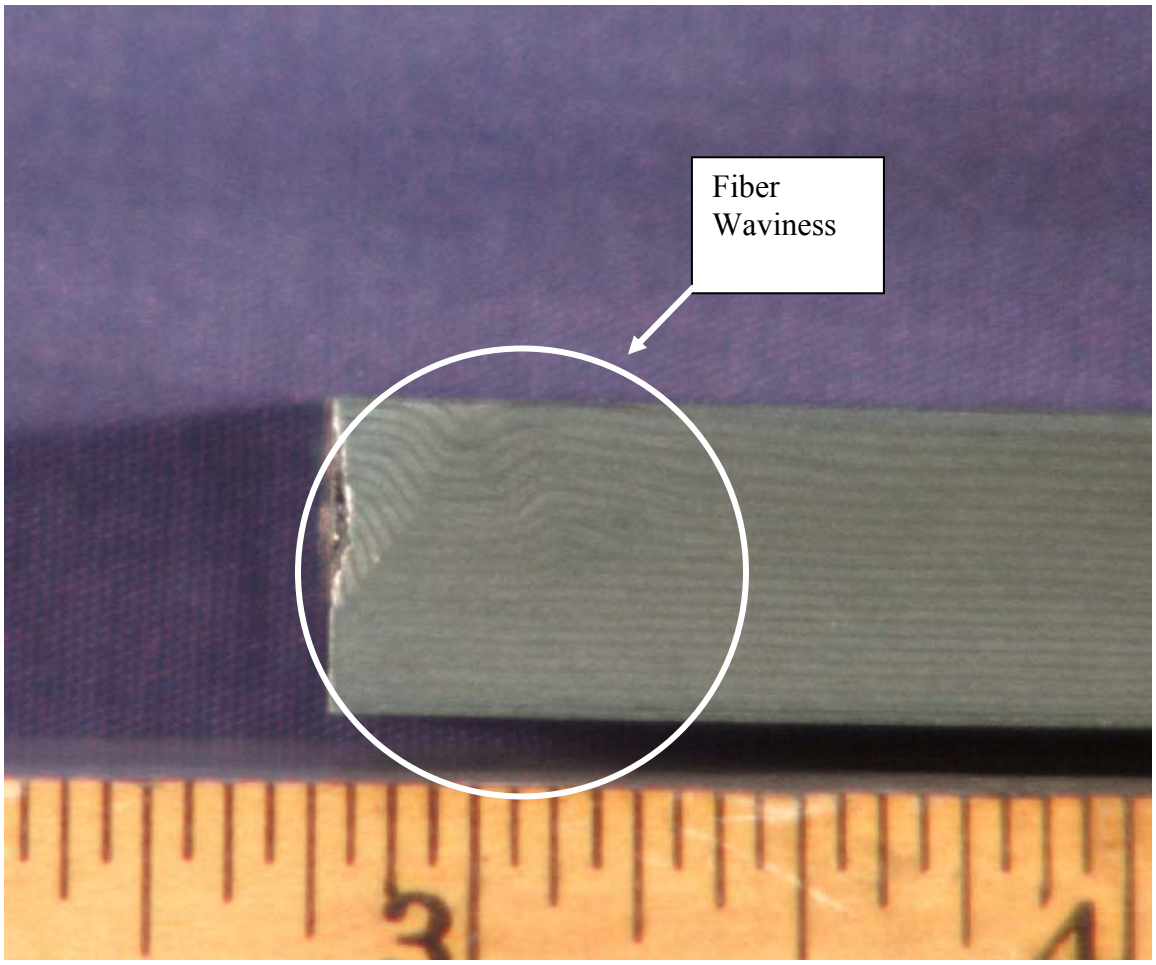

Figure 1. Photograph of edge of sample 121202-3-2 showing wave in fiber layers.

In addition to the samples previously mentioned, 3M Corporation provided a portion of an AlMMC tube that had been destructively tested. Fiber misalignment (or waviness) was noted on the end of the sample portion. A photomicrograph of the polished end of the sample, labeled

3MC1, is shown in figure 2. The dark striations are the longitudinal layers and the lighter bands are the hoop wraps. This sample was included in the NDE tests with the other samples.

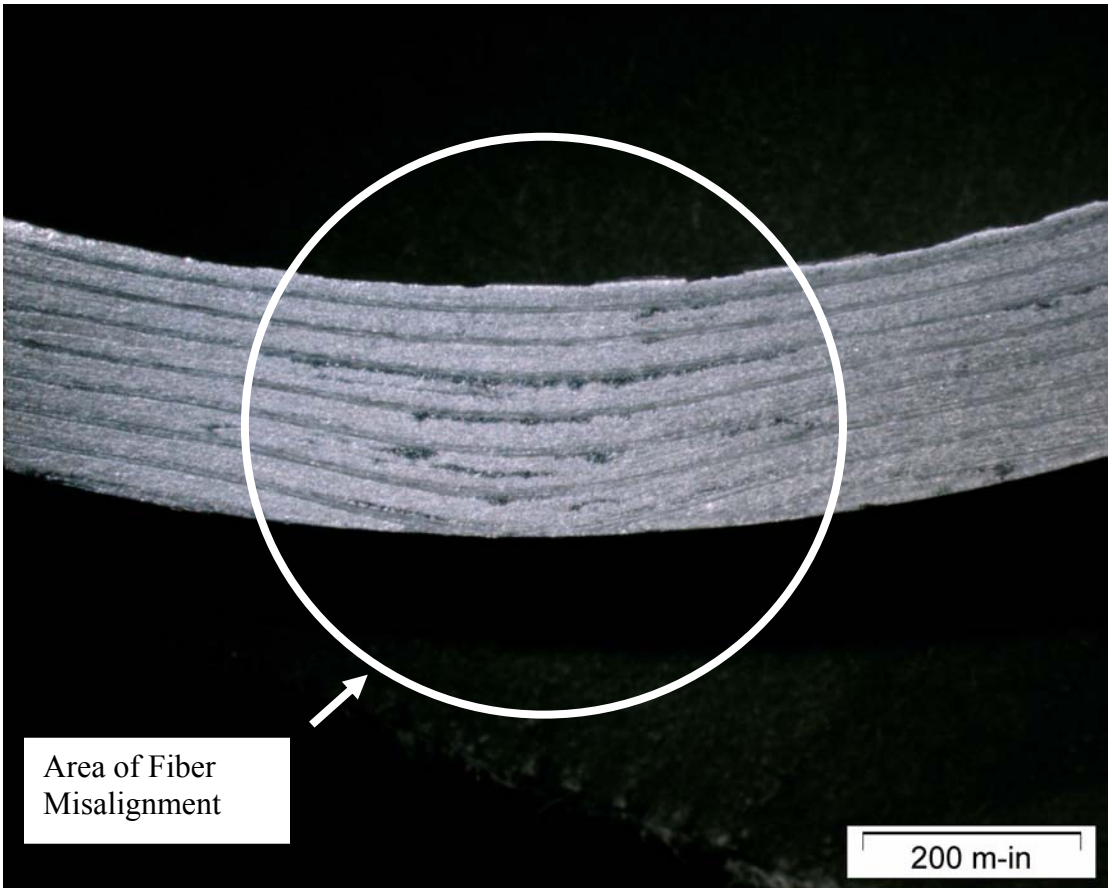

Figure 2. Polished end of sample 3MC1 showing fiber misalignment.

4. Ultrasonic Experimental Approach and Initial Results

4.1 Initial Considerations

The U.S. Army applications of AlMMCs for immediate consideration are an artillery shell and a composite mortar tube. A prototype AlMMC artillery shell has been demonstrated (Hoppel, 2002), but the use of AlMMC in a gun tube is still being developed. Other applications will undoubtedly arise as the material gains greater acceptance and the price comes down. For the present purposes, focus will be placed on the types of flaws that will be critical for these types of applications. Specifically, the NDE techniques will need to be able to detect gross defects such as delaminations, large cracks in the matrix, areas of low fiber content, lack of infusion, and large degrees of porosity. Of lesser concerns are the detection of inclusions, contamination, broken fibers, and microscopic cracking.

One of the most simple and obvious NDE techniques that has been used in the past is visual examination. This technique can be used successfully when flaws such as cracks or delaminations intersect the surface of the part. One of the flawed parts described in table 3 had a region of poor metal infiltration near the surface, causing the machined surface to be quite rough. The defect was clearly visible to the naked eye. Fiber waviness is also quite evident, especially in several AlMMC cylinders that were machined so that alternating fiber layers intersected the surface to give the surface a "wood grain" appearance.

Another simple NDE technique is a determination of density. During the course of this investigation, the University of Delaware provided AlMMC cylinders to ARL. One of these cylinders, labeled UDEL No. 3, was weighed in both air and water. The values were 1003.8 and 695.1 g, respectively. The temperature of the water at the time of the weighing was 22 °C. Using the density of water at this temperature (0.9978 g/cm^3), the calculated density is

$$1003.8/(1003.8\text{-}695.1)*0.9978 = 3.24 \text{ g/cm}^3. \quad (1)$$

Given that the density of the aluminum matrix is 2.7 g/cm^3 and the density of the fibers is 3.90 g/cm^3 (Fick, 2003), the fiber volume fraction can be calculated from the rule of mixtures to be 44%. This density measurement shows that the fiber volume fraction is significantly lower than expected.

4.2 Ultrasonic Measurements and Experimental Setup

Standard procedures were used for making ultrasonic measurements on the AlMMC specimens. These procedures will be reviewed briefly to clarify how the data were obtained and indicate possible sources of error.

The ultrasonic equipment is shown in figure 3. It consists of a water bath, an ultrasonic probe mounted on an arm, a three-axis motorized position controller for the arm, and a motor control unit that is governed by instructions from the software package. The software package used for this work is Ultrawin* written by Physical Acoustics Corporation, Princeton, NJ. The mode of operation was pulse-echo. That is, the transducer acted as a transmitter of the ultrasonic signal and also as the receiver of the echoes. Figure 4 shows a close-up of the ultrasonic probe and AlMMC sample. In all cases, the ultrasonic pulse was transmitted through the smallest dimension of the sample (i.e., its thickness).

A 5-MHz transducer was chosen for this work. A 10-MHz transducer was tried initially, but the signal attenuation was too great for this transducer to be of value. The resolution of the 5-MHz transducer signal is adequate to detect small flaws in the AlMMC material. If the smallest flaw to be detected is on the order of the wavelength of the signal (λ), then the relationship between the frequency (f), wave speed (c), and λ gives the smallest flaw-size detectable as $c/f \sim 8 \text{ mm } \mu s/5 \times 10^6 \text{ Hz} \sim 1.6 \text{ mm}$ or ~ 0.06 in. The resolution is also determined to some

* Ultrawin is a registered trademark of Physical Acoustics Corporation.

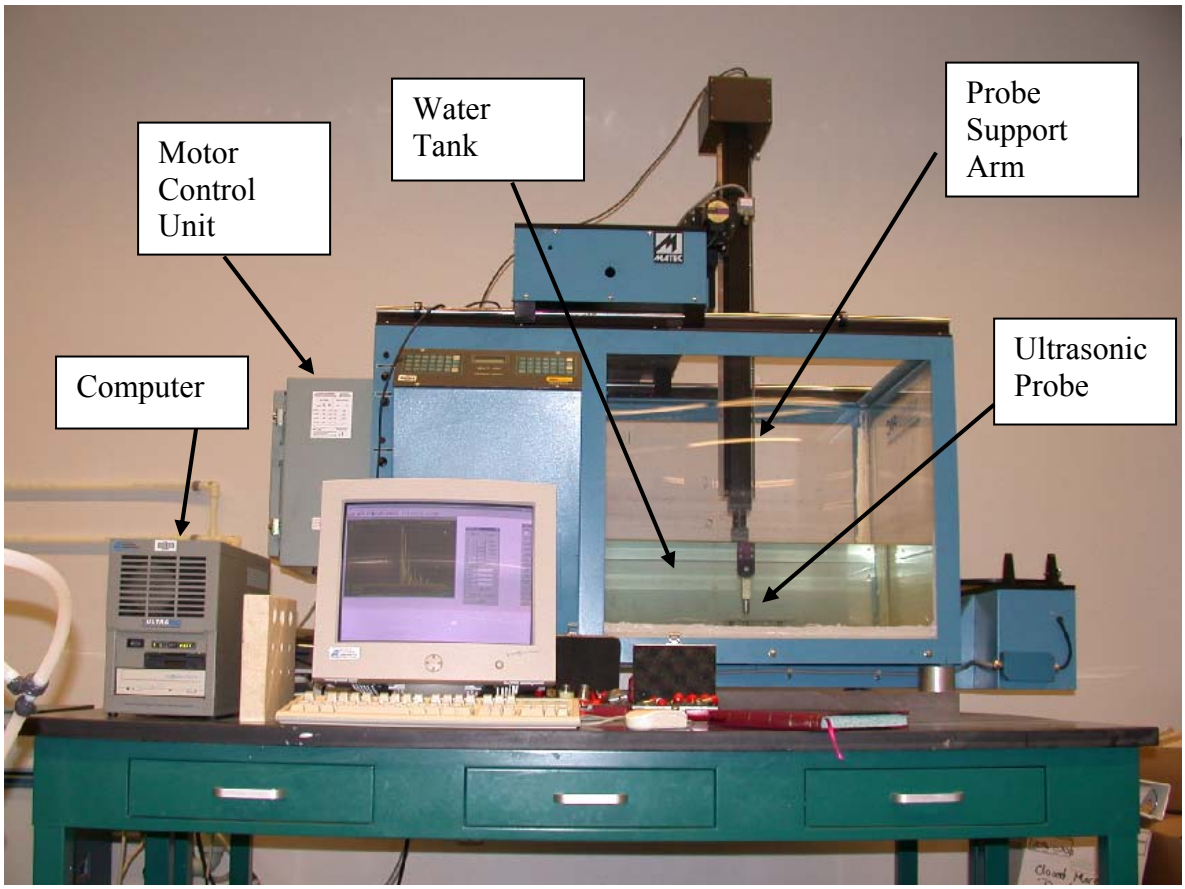

Figure 3. Ultrasonic scanning equipment.

extent by the physical dimensions of the transducer itself. The transducer was passed across the edge of an aluminum plate, and the amplitude of the second echo was measured. Figure 5 shows a plot of the normalized amplitude measurements vs. the transducer position.

The results indicate that the transducer can detect a large change in density with the resolution of ~2 mm. That is, between the 10% and 90% detection levels, the transducer position changes ~2 mm.

An example of an echo pattern obtained for an AlMMC sample is shown in figure 6. The first peak is the echo reflected from the surface of the material. The second peak has traversed the sample thickness twice, the third peak four times, and so forth.

The software allows two gates to be placed anywhere in the echo pattern. For this work, a gate was set up over the expected location of the second echo. (The first echo does not interact with the interior of the sample and therefore cannot be used for internal flaw detection.) There are two detection modes that can be used in conjunction with the gate. The one selected for this work was peak detection. In this mode, the peak with the highest amplitude within the gated region is selected for measurement. The time duration that the gate is open can be increased or decreased to ensure that the entire peak is contained within the gated region.

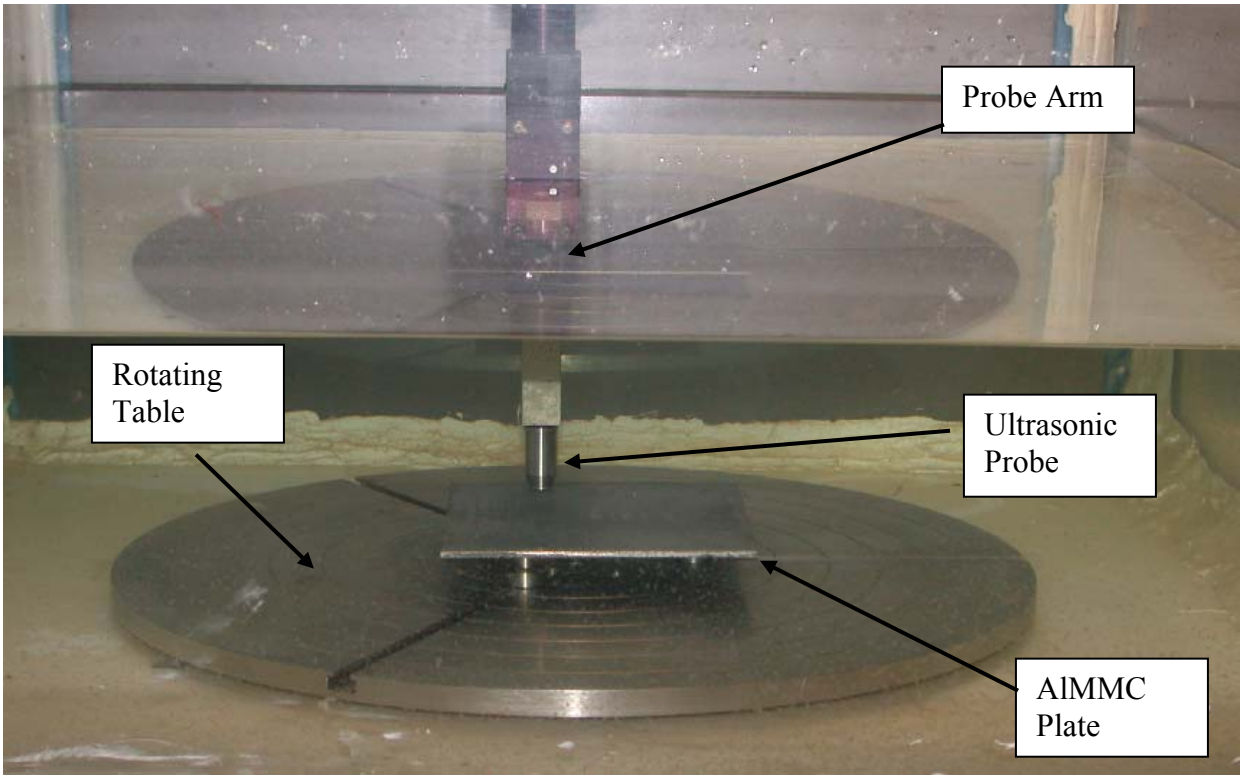

Figure 4. Normalized signal amplitude vs. transducer position.

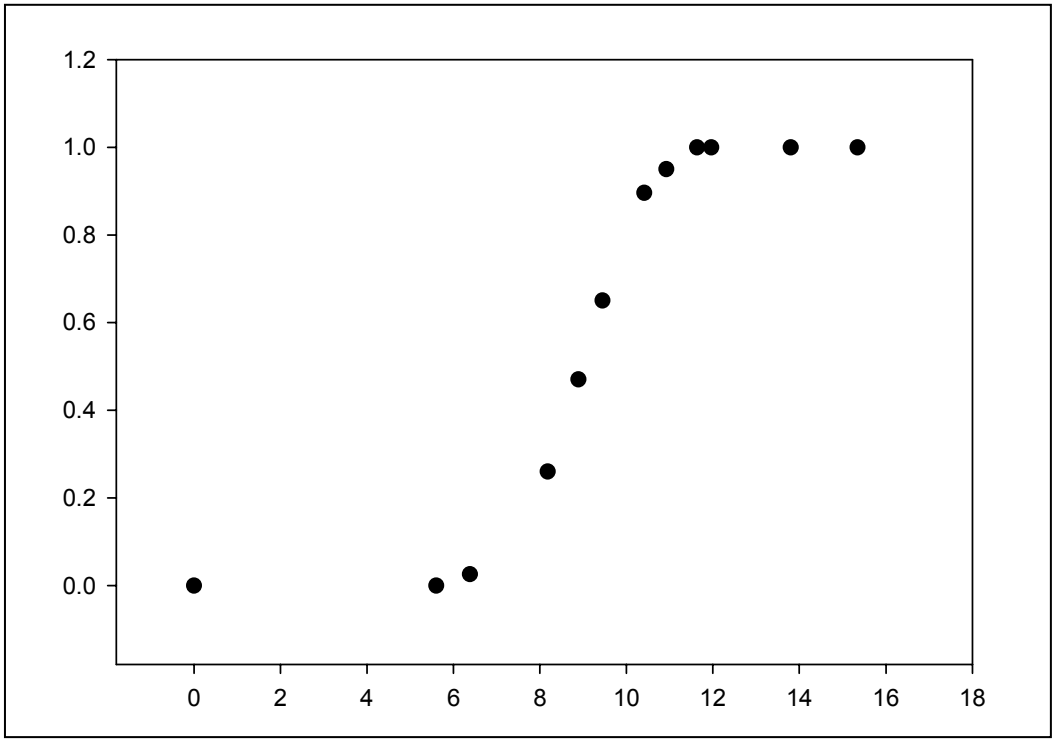

Figure 5. Normalized signal amplitude vs. transducer position.

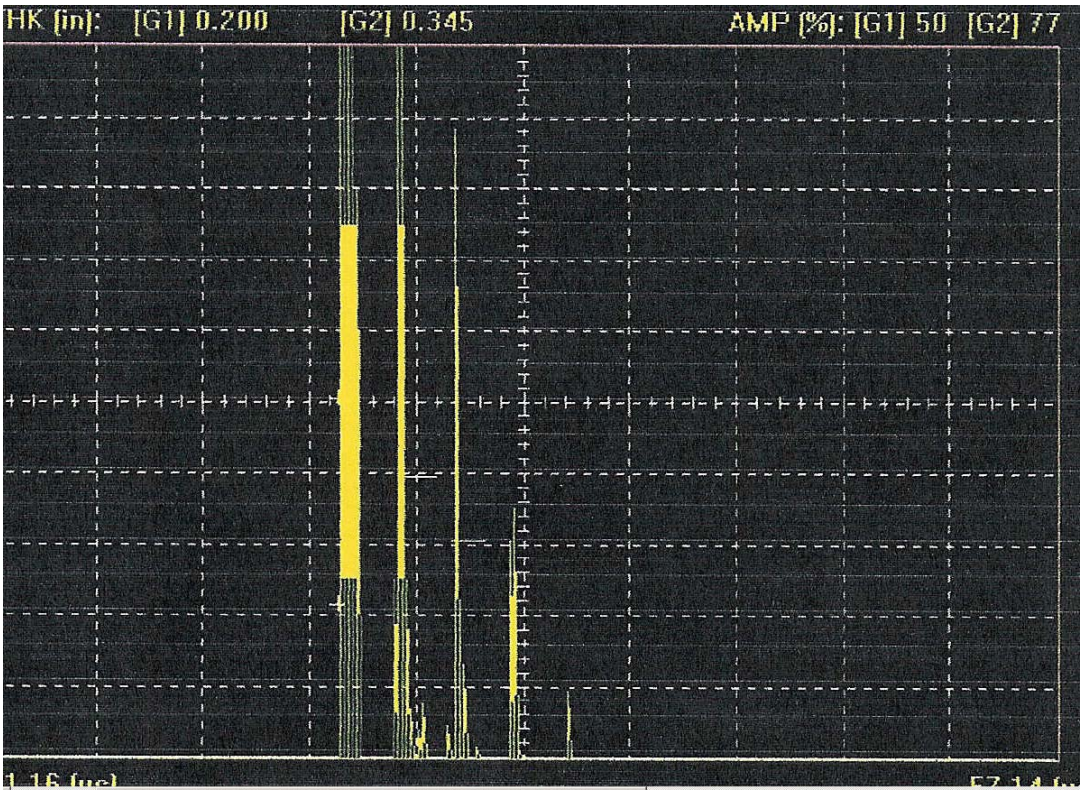

Figure 6. Echo pattern for a 5-MHz signal traversing an AlMMC sample.

The C-scan is produced by moving the transducer in a pattern that rasters over the entire sample. The peak amplitude for the gated echo is measured at discrete points, and a color code is used to display the data in a two-dimensional picture. Normally, a defect in a material will cause a loss in signal amplitude. Thus, defects are indicated by low signal returns. Clearly, the procedure is qualitative in nature, and defects are detected through differences in signals. Also, the nature of the defect (inclusion, delamination, fiber waviness, etc.) is not indicated.

The gate can be triggered in two ways. For this work, the gate was triggered from the signal associated with the first echo. Because the gate is open for a certain time duration, a change in sample thickness may result in the selected echo moving out of the gated region. In this case, the detected peak amplitude may decrease to zero giving a false positive for defect detection. Consequently, it is important to have either a gate that has a large time span or a sample with uniform thickness throughout the region that is being scanned.

4.3 Ultrasonic Examination of AlMMCs With Known Flaws

4.3.1 Lack of Infusion Flaw

C-scans were performed on four of the five samples received from 3M Corporation plus the partial cylinder made from AlMMC. The first sample examined was 112202-1-2. The scan for this sample is shown in figure 7.

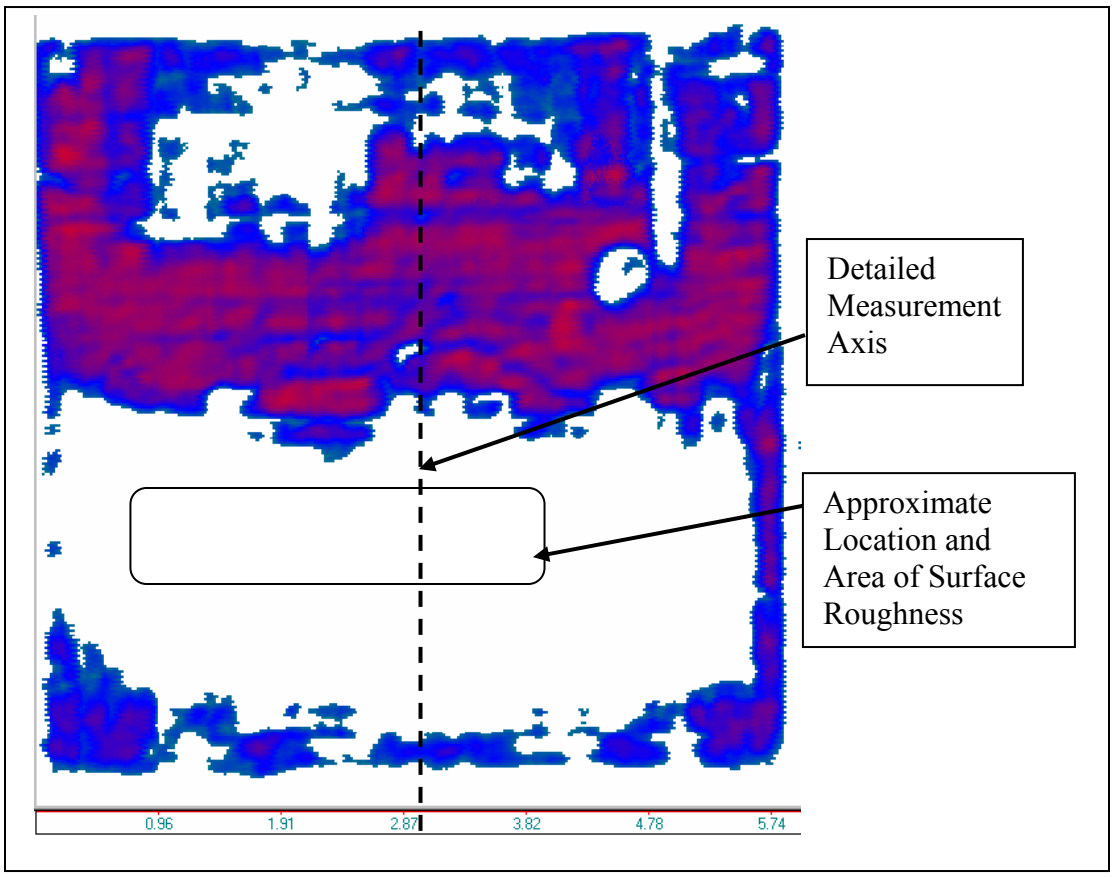

Figure 7. C-scan of sample 112202-1-2.

In this figure, the red indicates a strong return signal, the blue represents a weaker return, and the white indicates a very low return. Thus, there is a good possibility that some type of flaw is located in the white area. In fact, the surface roughness of this plate (even after machining) was an indication that the fibers had not been completely infused with aluminum. This area of surface roughness is shown in figure 8 as an overlay to the C-scan. It is considerably smaller than the total area shown by the C-scan to have a potential defect. The transition from the area indicated by blue on the C-scan to the white area was investigated in a more quantitative manner. Individual measurements of the sonic velocity and second peak amplitude were taken along the broken line shown in figure 7. The equation of this broken line would be x = 3 inches in a coordinate system where x = y = 0 is the bottom left-hand corner of the plate. A plot of the second peak amplitude vs. position along the measurement axis is shown in figure 8. There was virtually no signal (first peak amplitude) between y = 0.5 in and y = 2.8 in. The drop-off in signal going from y = 3.2 in to y = 2.9 in is almost as steep as that shown in figure 6, indicating an abrupt discontinuity in material properties.

It was also noticed that there appeared to be some correlation between the second peak amplitude and the sonic velocity. The sonic velocity was determined by measuring the transit times of the second through third echoes, taking an average, and dividing that time into twice the sample

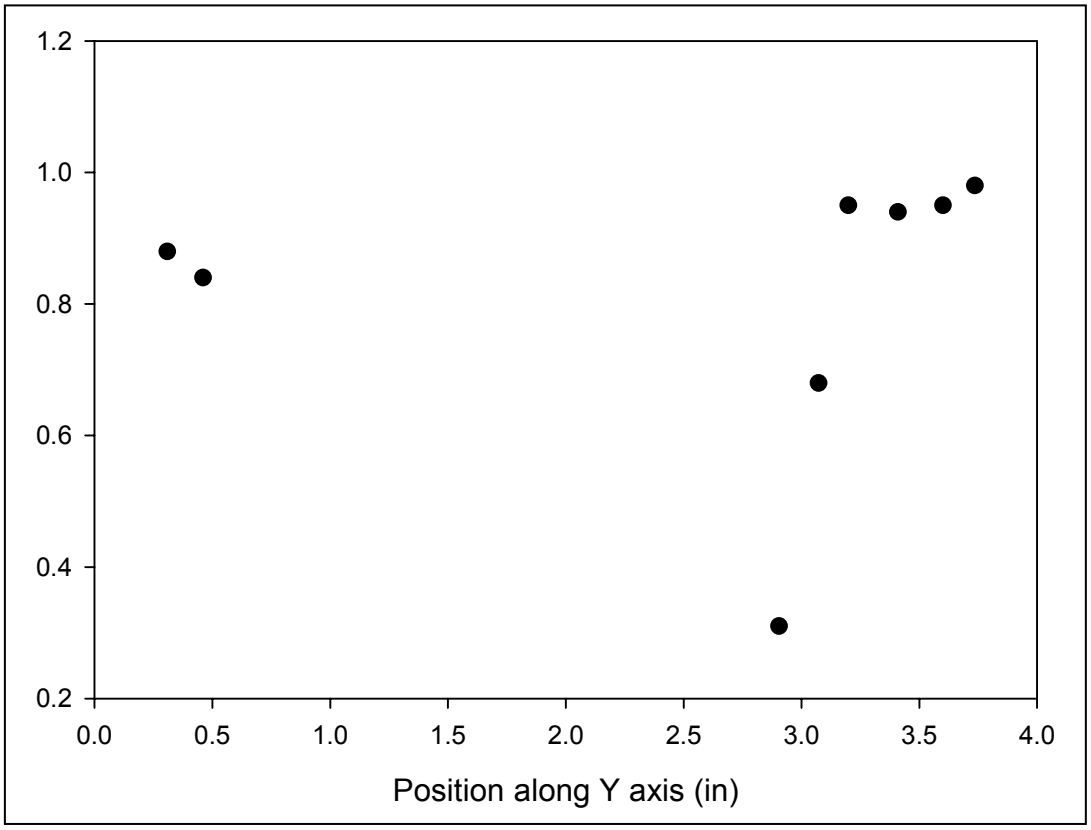

Figure 8. Peak amplitude of the second echo as a function of position along the measurement axis.

thickness. In the case where the peak amplitude was too low to obtain an average from three echoes, no velocity was determined. The results are shown in figure 9.

Except for the one outlying point, there appears to be a rough linear relation between the sonic velocity and peak amplitude. The low value of the amplitude for the outlier might be due to the surface roughness, dispersing the incident sonic wave and thus reducing the amplitude of subsequent echoes.

The plate was cut along the measurement axis to reveal the internal structure of the composite material. High-magnification photographs of two regions are contrasted in figures 10 and 11. In figure 10, the portion of the sample where the ultrasonics indicated a sound material is shown. This figure reveals alternating layers of fiber material with even spacing between layers. Figure 11 shows a small portion of the region where problems might be expected from the ultrasonic measurements. This photomicrograph in this figure appears to be slightly out of focus. This is due to the uneven nature of the polished surface. That is, there are portions of layers where only fibers are present with no aluminum matrix. In some areas fibers are missing, possibly removed during the polishing process. It is clear that this is the portion of the sample where there is a lack of infusion.

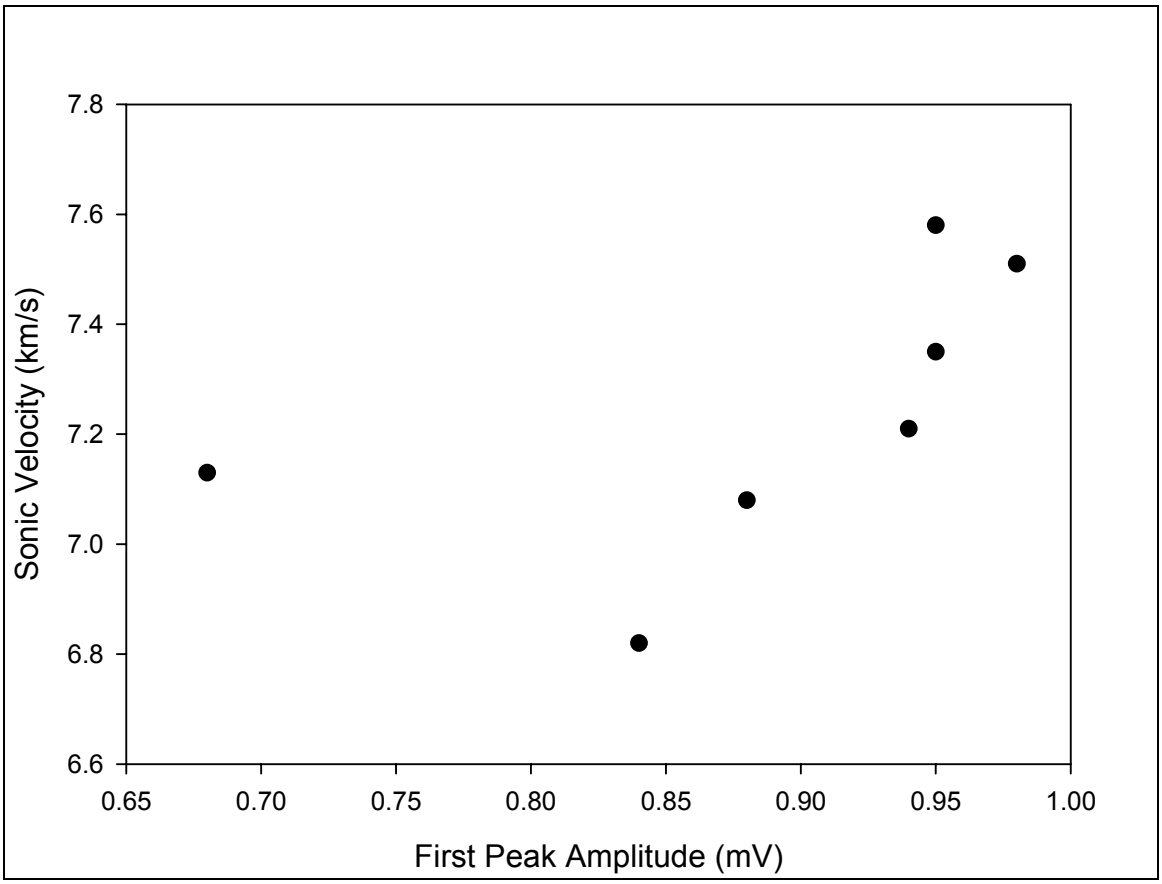

Figure 9. Sonic velocity vs. peak amplitude along the measurement axis.

A visual examination with a low-power magnifying glass of the cut and polished surface revealed delaminations or lack of infusion from ~ y = 0.5 in to y = 2.75 in. This corresponds to the white region in the C-scan for this sample.

4.3.2 Waviness Flaw

Two samples were examined that had fiber waviness or misalignment. A C-scan of sample 121202-3-2 is shown in figure 12. The scale shown in the bottom of this figure is in inches and is applicable only to the horizontal direction. The sample is ~6.1 in long. A small strip at the right-hand edge of this sample was machined thinner than the remainder of the sample. Consequently, there was no return signal within the gated area for this portion of the sample.

This figure shows the area where the fiber waviness is observed, extending ~3/8 in along the left edge of the sample (see also figure 1). While this portion of the C-scan has a somewhat weaker return signal than other portions of the sample, it certainly is strong enough to suggest there is no significant defect in that region. There also appears to be a more serious defect indicated by the white area in the middle right-hand portion of the sample. The sample was sectioned perpendicular to the long axis of the sample through a location that would reveal what sort of

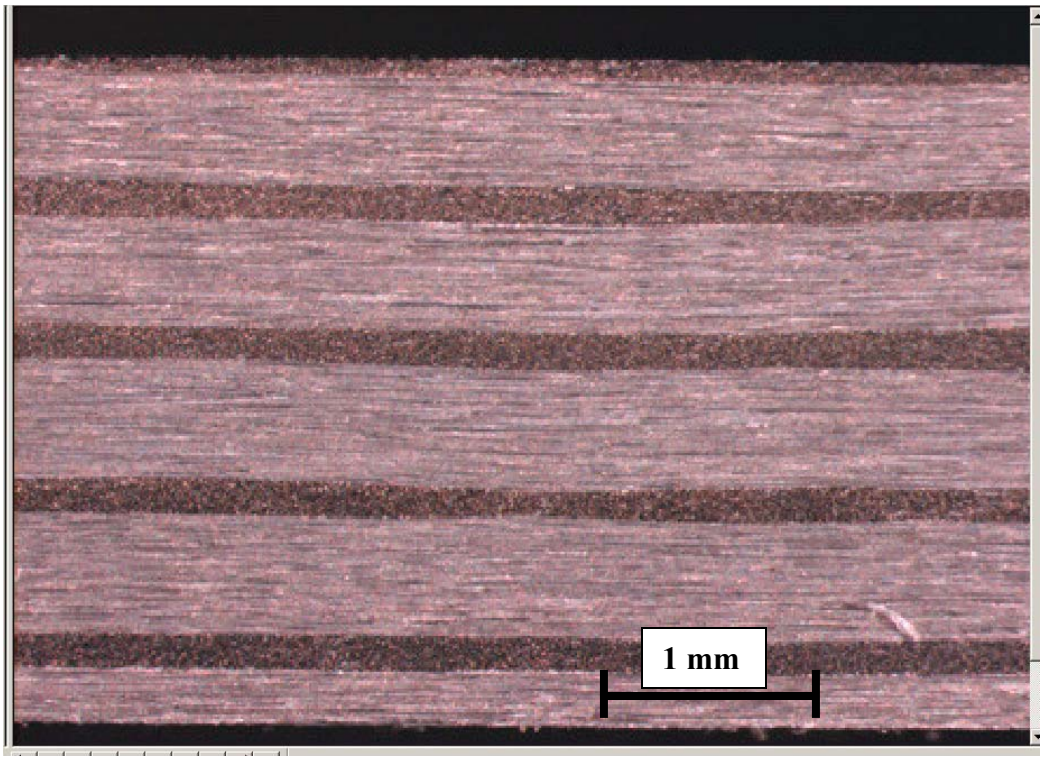

Figure 10. Photomicrograph of sound material portion of sample 112202-2-1 (through-thickness cross section).

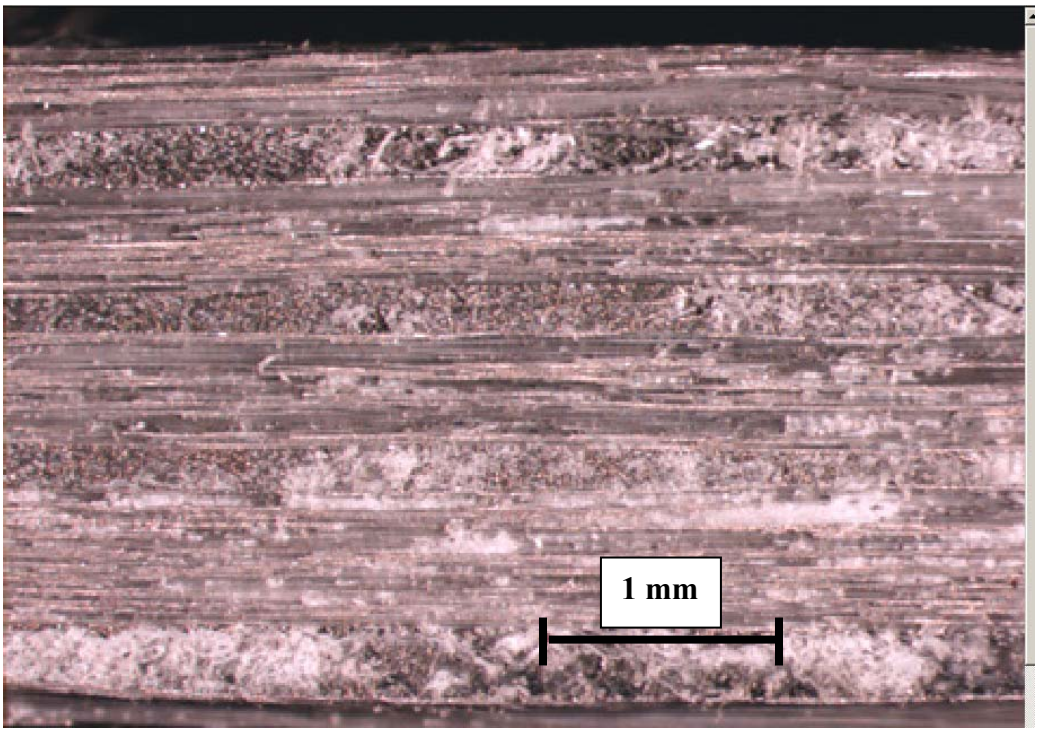

Figure 11. Photomicrograph of unsound portion of sample 112202-1-2.

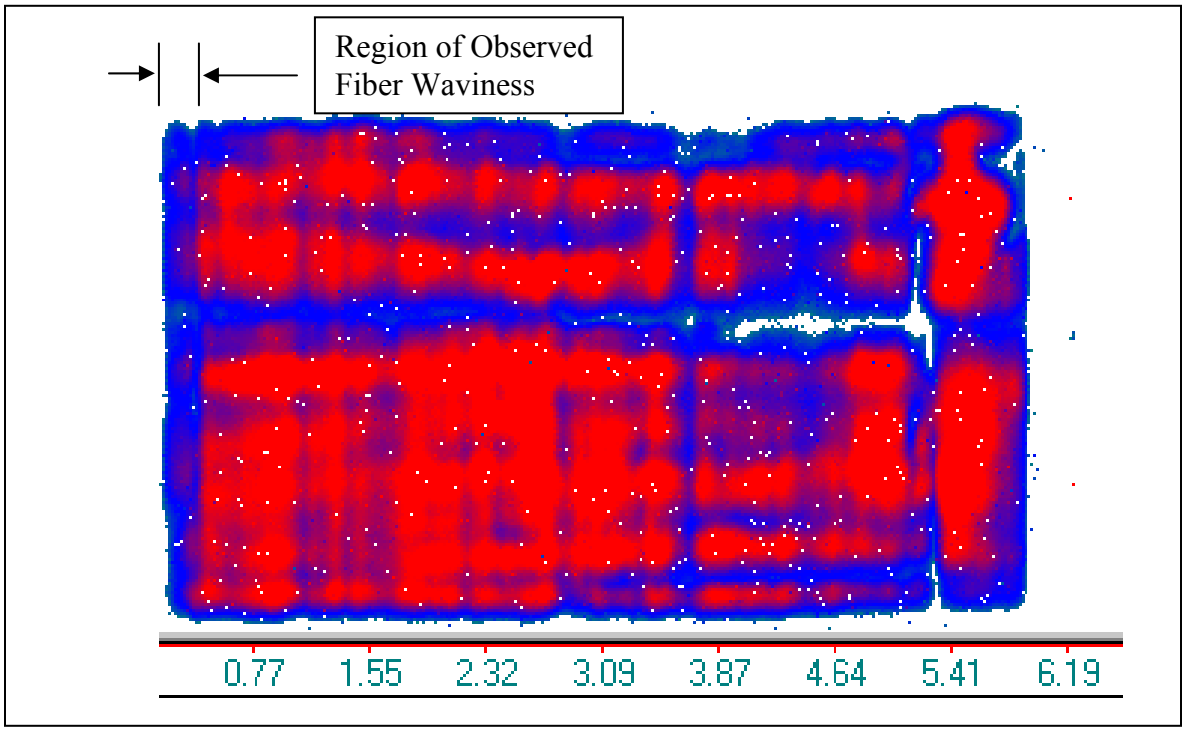

Figure 12. C-scan of sample 121202-3-2 (fiber waviness).

defect was represented by the white area in the C-scan. However, no defect of any significance could be observed in this location.

A second sample of waviness in the fiber layers was found in the partial cylinder sample provided by 3M Corporation (see figure 2). It was labeled as 3MC1. The sample was in the form or an arc (~130°) that was 0.94 in wide and 0.20 in thick. The C-scan of this sample is shown in figure 13. The scale at the bottom of this figure is in degrees. The waviness occurs from ~28–40°. There is no indication from the C-scan that there is a significant defect located in this region. (The blue portion of the C-scan is attributed to edge effects.)

4.3.3 Carbon Residue Flaw

The next sample examined (110102-2-1) had carbon residue as a known flaw. It was not clear at the onset how this defect would appear on the C-scan. Its C-scan is shown in figure 14. The scale at the bottom of the figure is in inches. The sample length was over 7 in. However, most of the C-scan signal is missing from ~6 to 7 in. There is also a flaw indication in a line running along the top of the C-scan. This latter flaw is attributed to the machining groove cut in the surface of the sample.

After polishing the edge of this sample, a closer look at the right-hand end revealed two cracks in separate planes extending about an inch into the sample from the right end. Figure 15 shows a photomicrograph of edge of this sample at the right-hand end.

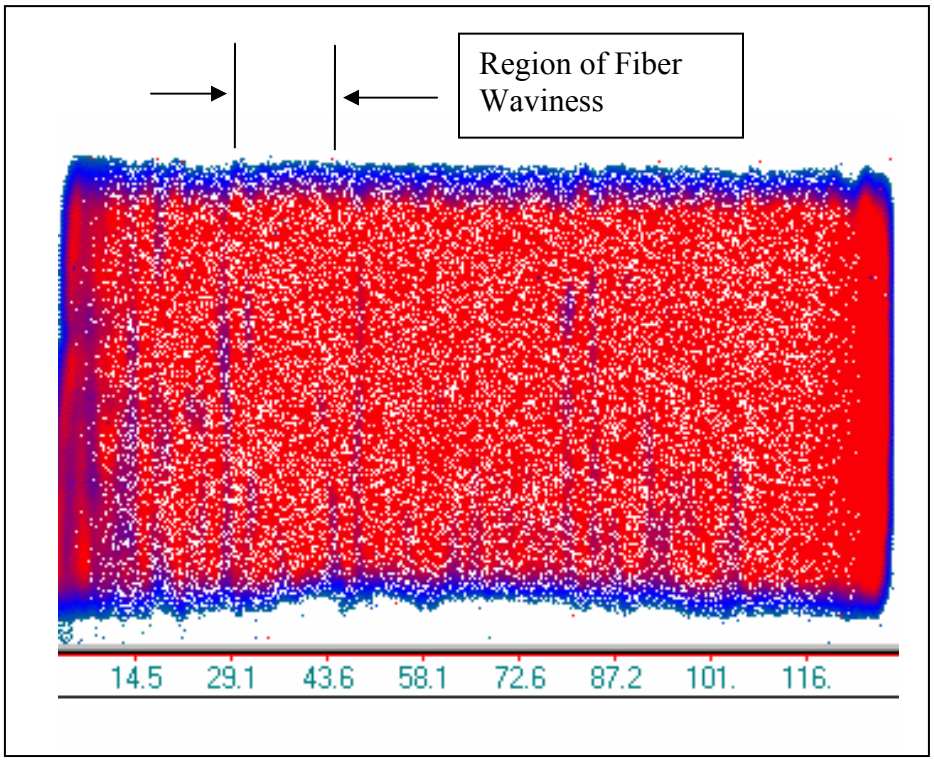

Figure 13. Carbon residue flaw.

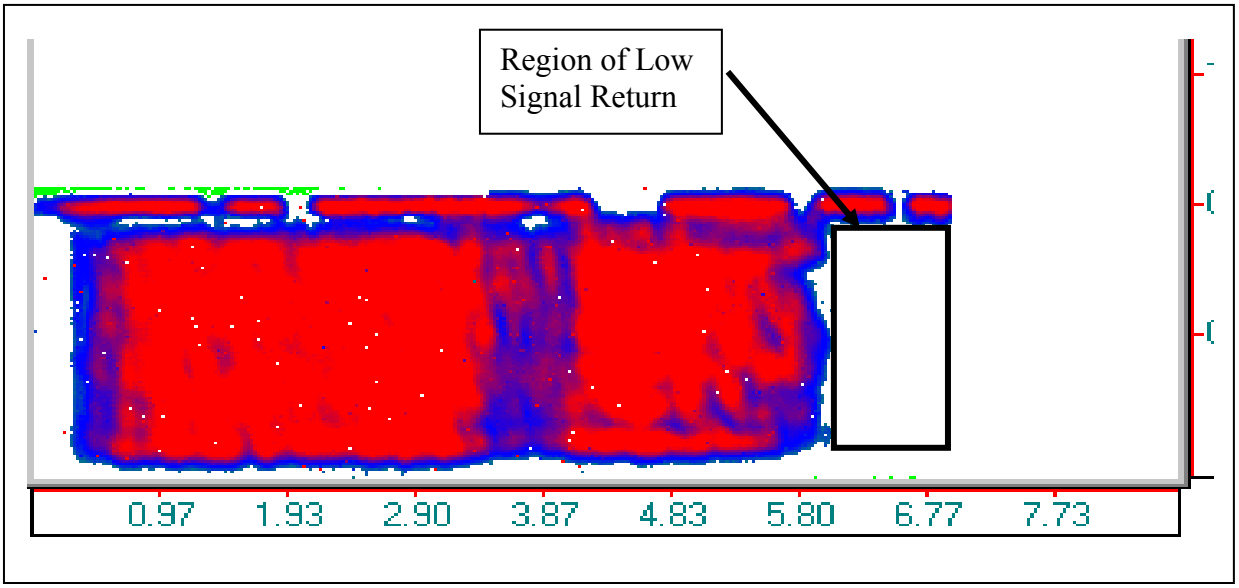

Figure 14. C-scan of sample 110102-2-1 (carbon residue).

4.3.4 Copper Intermetallic Flaw

The final sample with a known defect, 6243-1, was scanned with the result shown in figure 16. Note that the horizontal scale (in inches) does not apply in the vertical direction. There was no indication of any major defect in this sample.

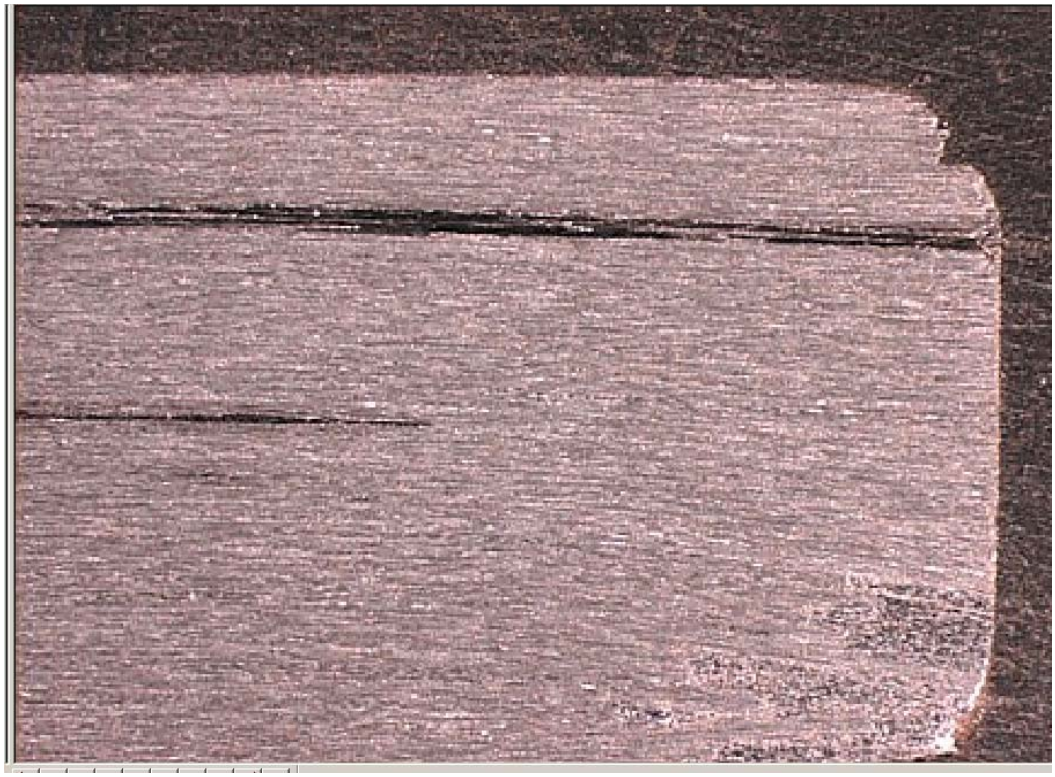

Figure 15. Photomicrograph of edge of sample 110102-2-1.

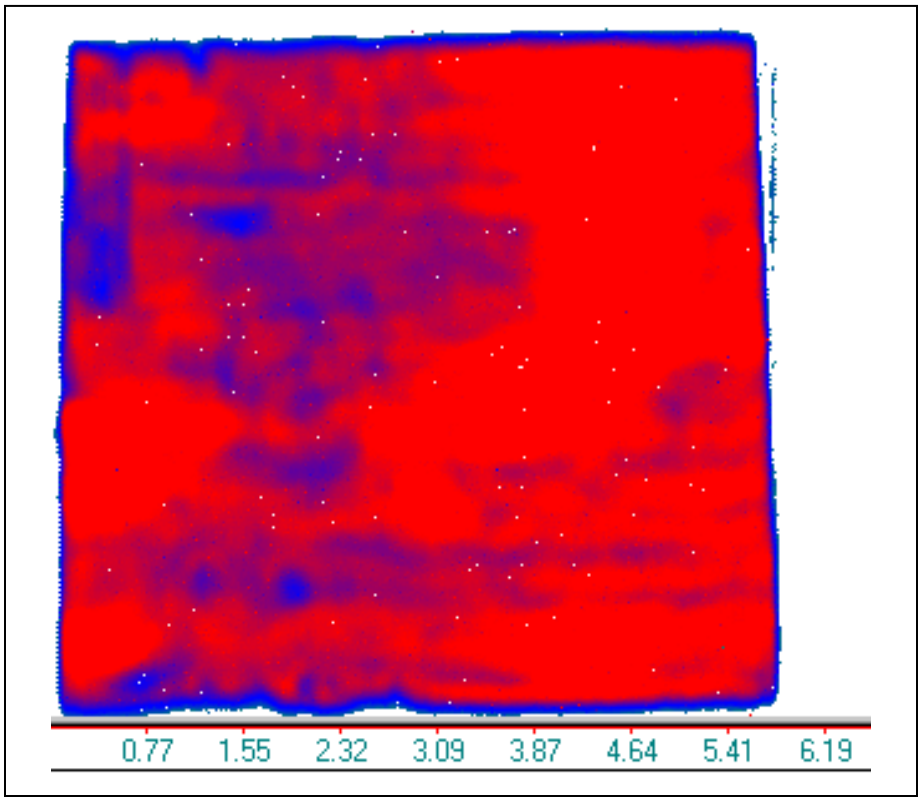

Figure 16. C-scan of sample 6243-1.

5. Meandering Winding Magnetometer Evaluation of AlMMC

5.1 Background and Theory

Eddy current measurements have been a useful nondestructive evaluation technique for metals for some time. The general idea behind this approach is to produce a current in a wire (driving coil) near the surface of a metal that induces eddy currents in the metal. This induced current produces a magnetic field that opposes the field produced by the drive coil. By sensing the induced current, measurements can be made to determine the local changes in the metal's electrical properties (conductivity and permeability). Those changes may be indicative of flaws in the metal.

Jentek Sensors has taken this technique to a higher level. They have solved Maxwell's Equations for specific situations to create databases of responses that allow the real-time conversion of sensor responses into actual values for material and geometric properties, such as conductivity and permeability. One of the keys to their approach is to design the drive winding and sensing coil so that the sensor response can be accurately modeled. In addition, the MWM hardware and software has been designed so that sources of error induced by the electrical circuitry in the equipment can be zeroed out in an efficient manner and still have long leads to the sensing elements. An additional advantage is that the system can be easily calibrated in air for some applications.

The solutions to Maxwell's Equations are put into databases of responses that, in two dimensions, can be displayed in the form of measurement grids that plot two calculated parameters in terms of the two measurement responses. In the current case, those parameters are conductivity and lift off (distance from the sensor to the surface of the sample). In order to determine these two parameters, two variables are measured. These variables are the magnitude and phase of the complex transinductance. The transinductance is equal to the transimpedance divided by $2\pi fi$, where f is the frequency (in Hertz) of the drive signal and I is the square root of minus one. The transimpedance is given by the sensing element voltage divided by the drive winding current (Goldfine et al., 2002). The transinductance expresses the inductive coupling between the drive winding and the sensing elements. The measurement grids are generated prior to data acquisition and cover the range of material and geometric properties expected during the measurements. Because the bulk of the model computations are done ahead of time, measurements of the sensor response can be converted into effective material and geometric properties in near real time by performing a table look up. In generating these solutions, it is assumed that the material under examination can be represented by a layered geometry. For basic measurements of two parameters, such as conductivity and lift off, the material under examination is typically taken as infinitely thick. This assumption is generally good for

high-frequency signal drives, where the imposed electromagnetic field does not interrogate the sample very deeply. However, if the part is relatively thin so that the sensor is also sensitive to the material thickness, the effective properties that are measured can be different from the true properties. In these situations, measurement grids that account for the material thickness or higher order databases (e.g., three or more dimensions) that allow three or more properties to be determined, such as material thickness, conductivity, and lift off, can be used. One of the grids used in this study is shown in figure 17.

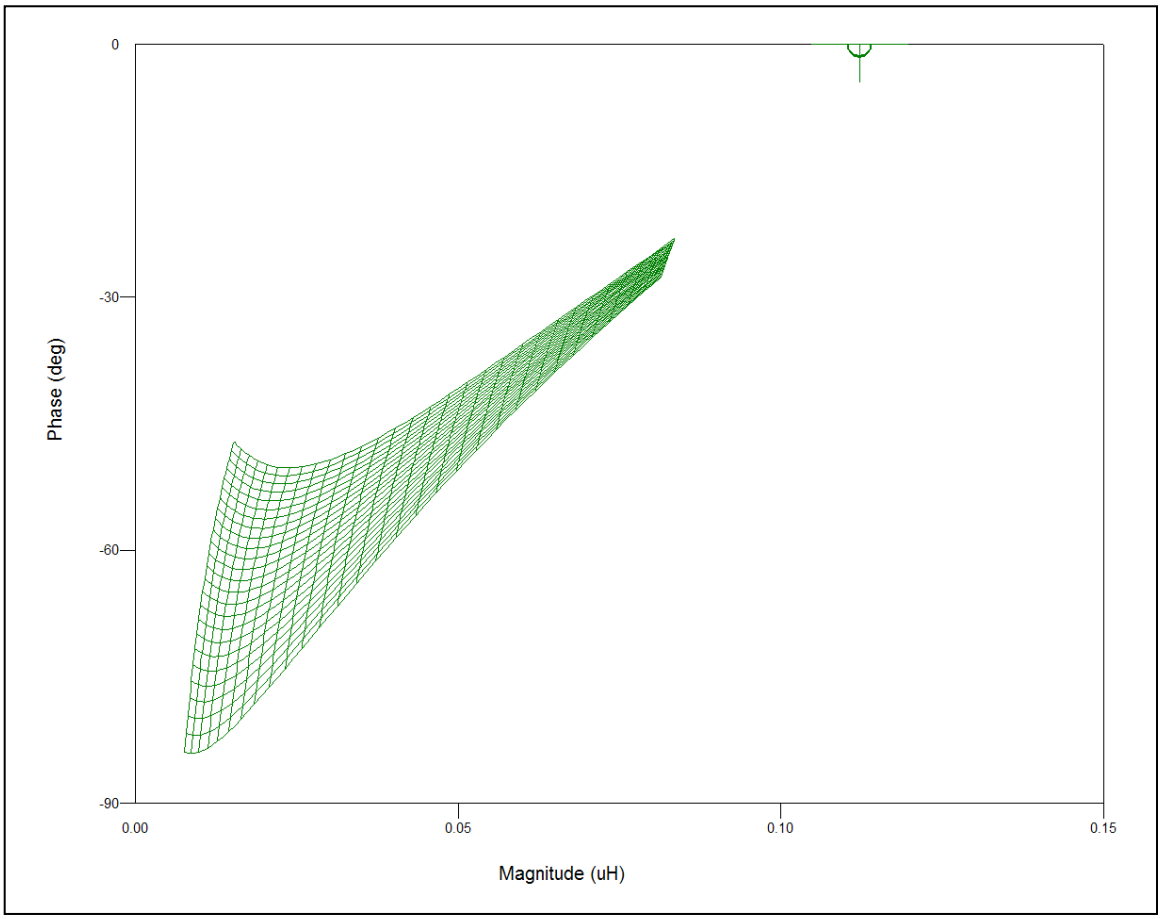

Figure 17. Solution grid used in this study.

Variations in the measured effective properties can reflect the presence of features or flaws in the material. When the flaw geometry is modeled by the geometry assumed for the grids, then the flaw can appear in only one of the effective parameters. For example, the feature can appear as a deviation in the conductivity alone if it is relatively thick and larger than the sensor footprint. If it is relatively shallow and small compared to the sensor footprint, it can appear as a deviation in the effective conductivity and lift-off reponses. As another example, if a paint layer thickness is varying, then the lift-off response will change but the conductivity should remain constant.

The depth to which the electromagnetic field penetrates a given material comes out of the solution to Maxwell's Equations for the type of sensor used by Jentek. The strength of the magnetic field is proportional to exp $(-\Gamma_n z)$, where z is the depth into the material and Γ_n is given by (Goldfine et al., 2002) as

$$\Gamma_n = \left((2\pi n/\lambda)^2 + 2i/\delta^2 \right)^{1/2} . \quad (4)$$

Here, λ is the wave length of the drive coil, n is the harmonic number (an integer), i is the square root of minus one, and δ is given by

$$\delta = (1/\pi f \mu \sigma)^{1/2} . \quad (5)$$

In equation 5, f is the frequency of the drive signal (in Hertz), μ is the permeability of the material, and σ is the conductivity of the material. The penetration depth of the signal is given by 1 divided by the real part of Γ_n. The penetration depth is defined to be the distance into the sample where the drive signal drops to 1/e of its original strength. This penetration depth is not the depth of sensitivity though, because sensitivity to flaws is affected by such factors as (1) flaw size, geometry, and depth; (2) differences in flaw properties compared to the surrounding medium; (3) the noise level of the instrumentation; and (4) material inhomogeneities (e.g., grain-to-grain variations). As a very rough upper bound, the maximum depth of sensitivity is typically taken as three times the depth of penetration. Note that the penetration depth is more complicated that the traditional skin depth, given by equation 5. For high frequencies and conductivities, the traditional skin depth term dominates the penetration depth. For low frequencies and relatively large sensor dimensions, the first term in equation 4 dominates. This effect is shown in figure 18, supplied by Jentek Sensors. Here, the depth of penetration (DOP) is shown as a function of frequency for five different sensors and three values of conductivity. The conductivity values are in terms of the International Annealed Copper Standard (IACS), where copper is taken as 100. Thus, 30% IACS is the conductivity of a material that has 30% the conductivity of annealed copper.

For the work to be presented here, the sensing array FA24 was used. The software used with the system allowed measurement of conductivity for many frequencies, ranging from 6 kHz to over 100 kHz. In the current work, frequencies in the range of 15–100 kHz were used. From the data shown in figure 19, this frequency range corresponds to a DOP range of 50–100 mil for a low-conductivity (3% IACS) sample. Given that most of the samples examined were ~100 mil thick and the measurement grids that were used assumed that the material was much thicker than the DIP, the measured effective conductivity will be affected by the sample thickness. This error will generally lead to a reduction in the effective conductivity as the frequency is decreased and reflects the contribution of the nonconducting air on the back side of the material. The sensing elements in the flexible arrays are basically small loops that can be arranged in a line that can be swept over the surface of the part to obtain a C-scan of the material. There were 37 individual loops (or channels) on the sensor used for this work.

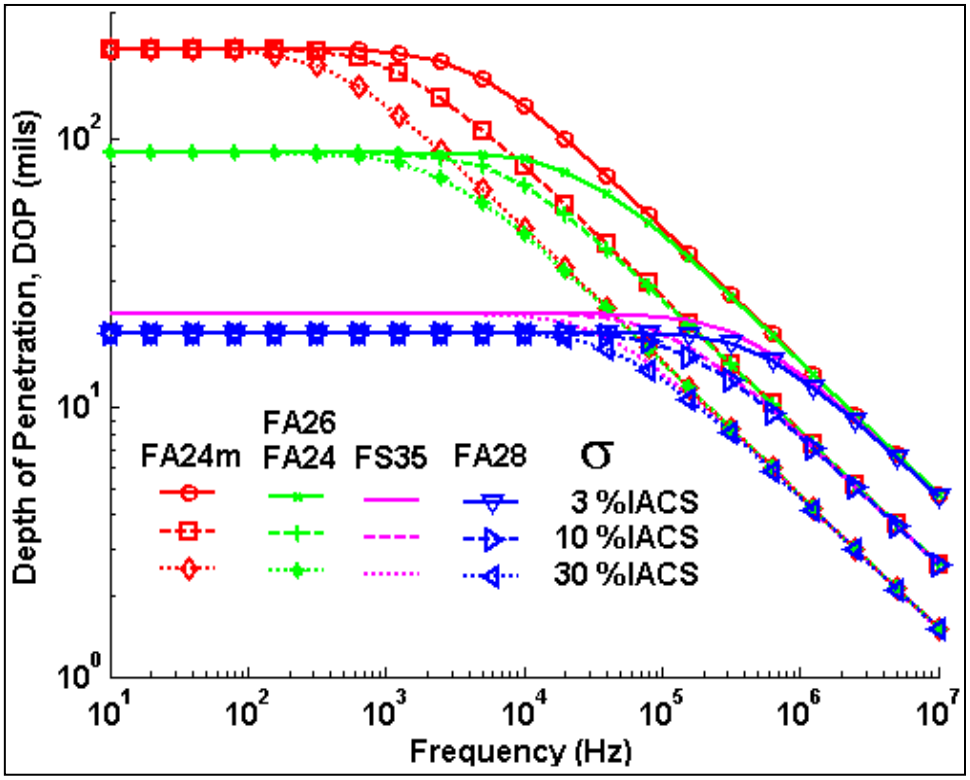

Figure 18. Approximate depth of penetration vs. frequency for one sensor (FS35) and four sensing arrays (FA24m, FA24, FA26, and FA28) (courtesy of Jentek Sensors, Inc.).

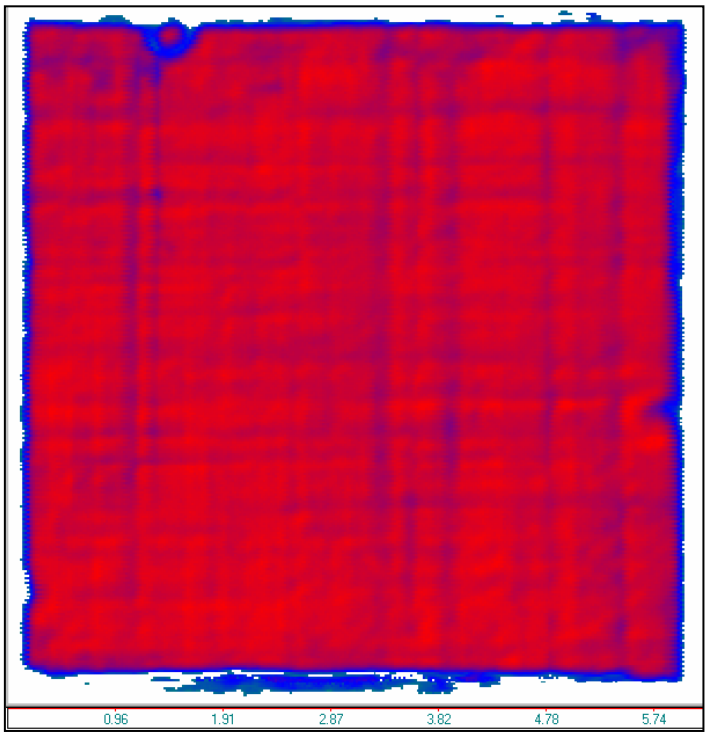

Figure 19. Typical C-scan of flat-plate AlMMC specimen from University of Delaware (sample 112502-1-1).

The loops covered a length of 3.66 in (93 mm), giving an average lateral span of 100 mil (2.5 mm) for each loop. The scan is aided with the help of a trolley that provides position information to the computer. There are choices offered by the software on how the signals from the individual channels are to be averaged and presented in the output. Software settings were chosen such that there was no averaging of the individual signals.

Appropriate grids and sensing arrays were supplied by Jentek Sensors to examine the AlMMCs. However, it must be understood that the work presented here is preliminary and is meant only to see what value there might be in applying MWM technology to detection of flaws in AlMMCs.

6. Application of Ultrasonic Measurements in Examining Flat-Plate AlMMC

Twenty flat plate AlMMC specimens were received from the University of Delaware for examination with both ultrasonic C-scans and the MWM scans. The plates were originally produced by the 3M Corporation. All plates had dimensions of ~6- × 6- × 0.1 in. The majority of the work involved ultrasonic measurements. The purpose of this work was to determine if the ultrasonic C-scans were capable of detecting significant flaws in AlMMC samples. (In this context, a significant flaw is one that would have a large effect on the mechanical properties of the material.) The plan was to have the plates mechanically tested (compression tests) at the University of Delaware so that a link between the NDE results and mechanical properties could be made.

Most of the plates received from the University of Delaware did not contain any indications that there were significant flaws present. A typical scan of one of these plates is shown in figure 19.

Even though the C-scan is fairly uniform, a faint cross-hatched pattern can be seen that is indicative of the fiber orientations (0 and 90°). A sample with a ±45° fiber layup is shown in figure 20. The cross-hatching is more pronounced in this sample. However, the return signal was strong, and there was no indication of any serious flaw.

Special attention was paid to those few samples that had indications of flaws. These particular samples were sectioned into coupons that contained the suspect areas in the gage section. An example of this is shown in figure 21 (courtesy of Ian Hall, University of Delaware). Here, a photograph of the sample 112002-1-2 is overlaid with the position and orientation of the test coupons. Included in the figure is the ultrasonic C-scan of the same plate. The white area in the scan is included in the gage sections of the two coupons taken from the middle of the sample.

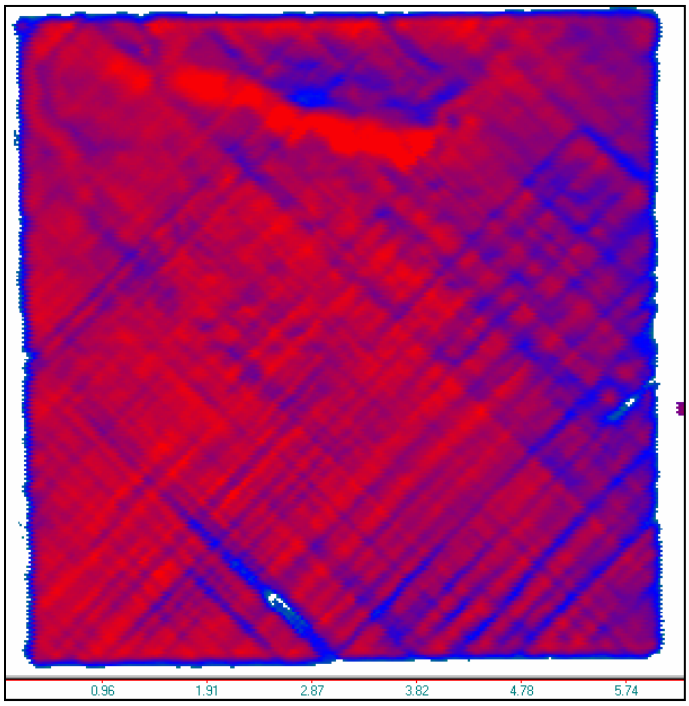

Figure 20. C-scan of sample 121602-2-1 indicating ±45° fiber layup.

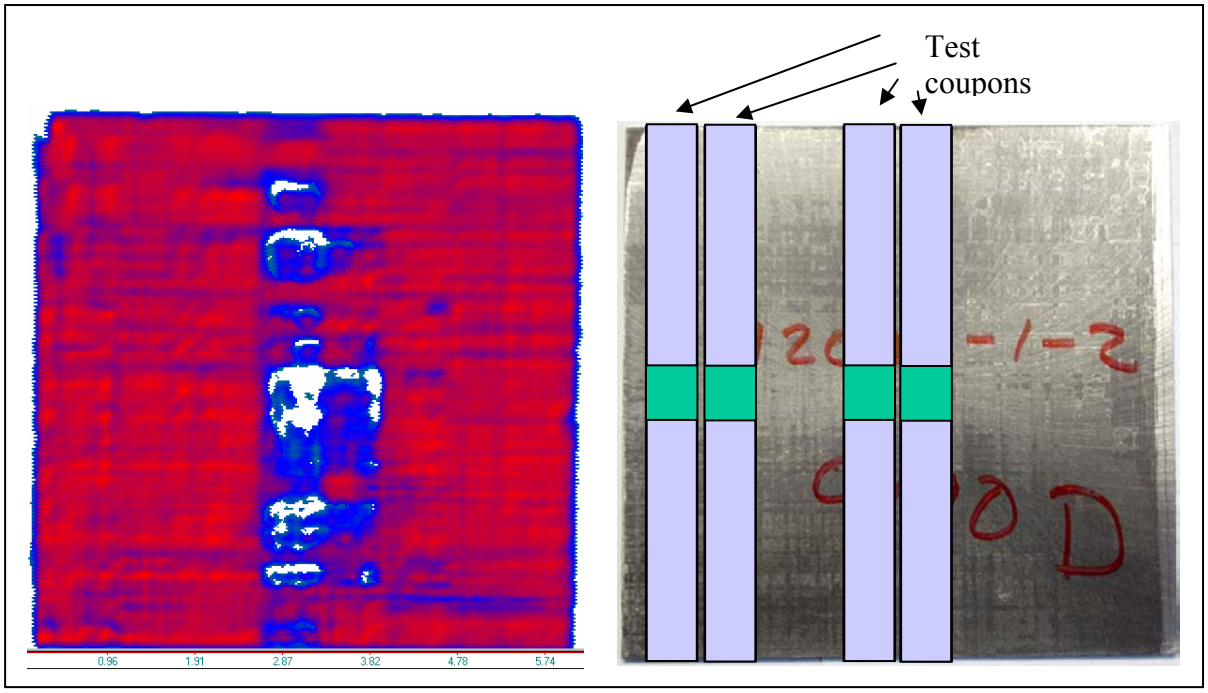

Figure 21. Comparison of ultrasonic C-scan with coupon location and orientation on sample 112002-1-2 (courtesy of Ian Hall, University of Delaware [Hall, 2003]).

None of the sectioned samples exhibited any crack, delamination, or lack of infusion as was seen in the samples with known defects. Several hundred micrographs of the suspect areas on various samples were taken with no indication of the presence of a gross flaw or defect. A micrograph of the central part of sample 112002-1-2 is shown in figure 22.

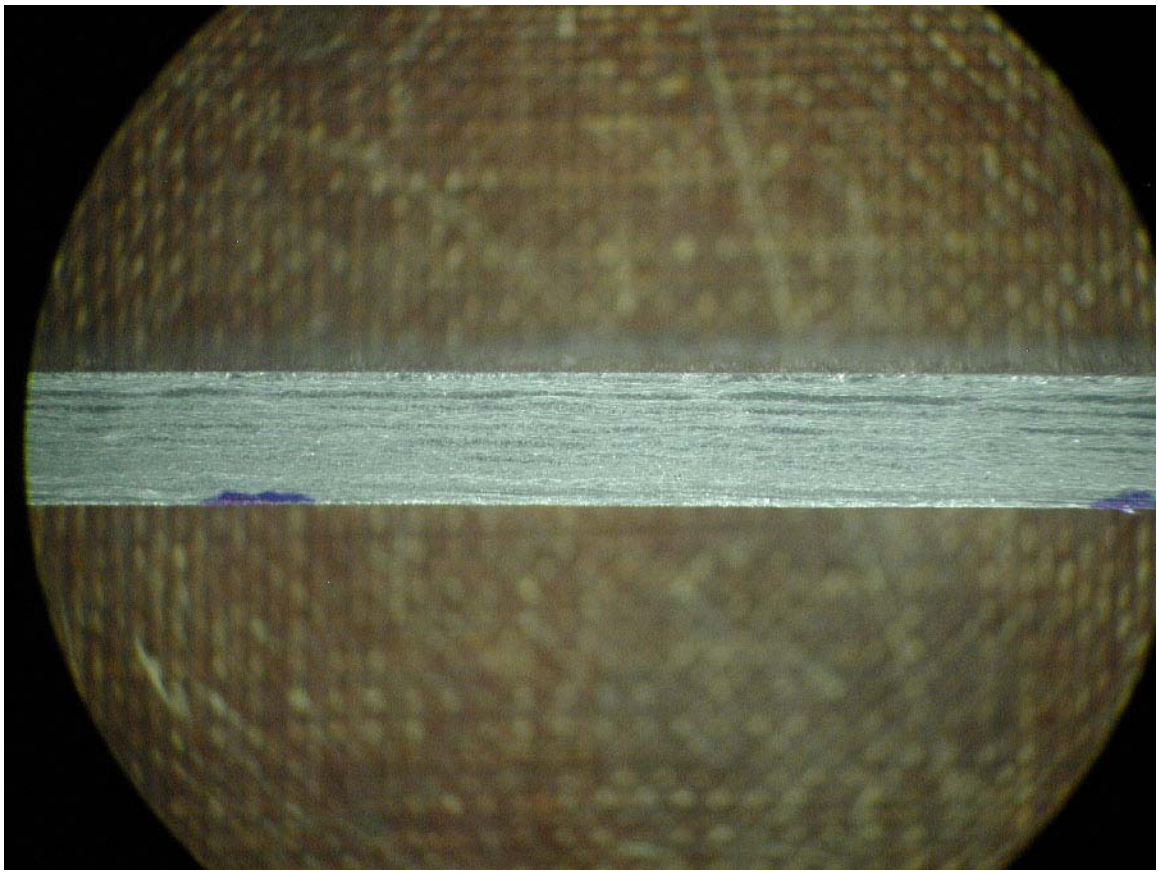

Figure 22. Micrograph of internal surface of sample 112002-1-2 (courtesy of Ian Hall, University of Delaware [Hall, 2003]).

The sectioned samples were tested in compression. Results opposite of what was expected were obtained. That is, samples made from areas where flaws were indicated (white areas) were the strongest, whereas samples made from sound areas were the weakest. Unfortunately, difficulties were experienced in designing end tabs for the test coupons that would provide consistent results in the mechanical tests (Bogetti, 2003). Research in this area is continuing.

An example of a C-scan showing possible flaws is shown in figure 23. Previous work indicated that a low (or nonexistent) signal return (shown as a white area in the scan) merited further examination. The scan in figure 23 has a large portion that is white. However, this scan was made with a low signal gain (20 dB). An identical scan with a higher signal gain (30 dB) results in the scan shown in figure 24. Here, the fluctuation in return-signal amplitude is similar (but not identical) to that shown in figure 23, but the signal strength is high enough so that no white

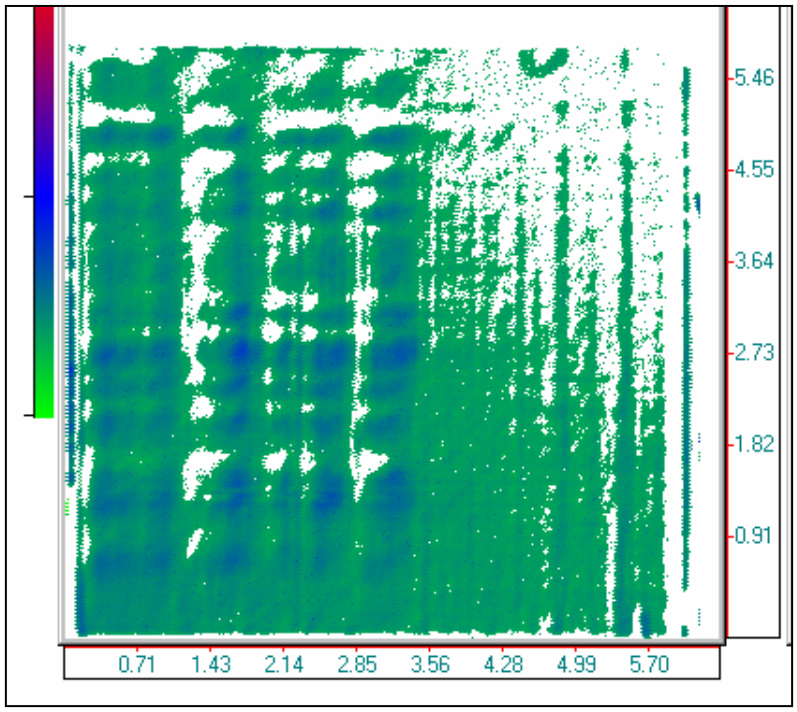

Figure 23. C-scan of sample 111902-2-2 showing possible flawed areas (20-dB gain).

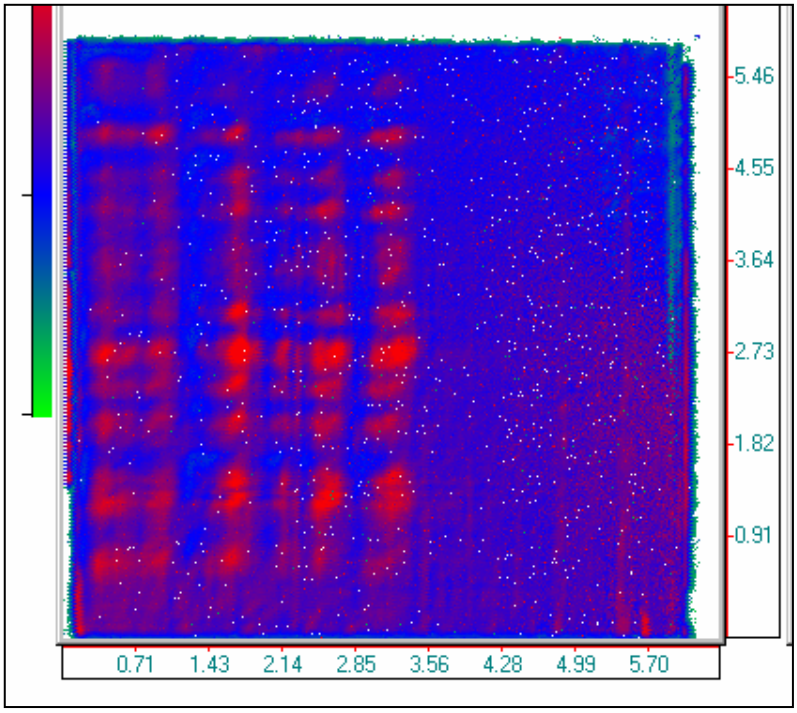

Figure 24. C-scan of sample 111902-2-2 at higher gain (30 dB).

areas appear. These figures are shown to emphasize the point that the C-scans as produced by the Ultrapac equipment show only relative changes in return-signal strength.

The source of the return-signal strength fluctuation was investigated by measuring the time of flight (transit time of the ultrasonic signal through the plate). A scan of the time of flight was made for the entire plate. This scan presents relative differences in the measured times of flight. However, those differences were hardly detectable with the color scale used. Absolute time-of-flight measurements were then made at four selected points and the sound velocity was calculated. Two of the points were in areas of high attenuation (low signal return), and two points were taken in areas of low attenuation (high signal return). In the areas of high signal return, four or five echoes were clearly distinguishable, whereas in the areas of low signal return there were only three echoes available for the measurements. Table 4 gives the results of those measurements. Included in this table are the corresponding values of the fiber volume content as obtained from equation 3.

Table 4. Ultrasonic velocity measurements.

Y Coordinate (in)	X Coordinate (in)	Attenuation	Ultrasonic Velocity (mm/μs)	Fiber Volume Content (%)
2.72	0.94	High	8.09	58
2.72	1.42	Low	7.63	44
2.72	1.77	High	8.27	63
2.72	3.05	Low	7.42	39

7. Discussion

Results of the literature search have been discussed in section 2. The general conclusion was that ultrasonics is perhaps the most useful approach to examine fiber reinforced composite materials for internal flaws. Therefore, most of the work presented in this report concentrates on this approach. In addition, a new technique called Meandering Winding Magnetometer was investigated to see what potential it has for flaw detection in AlMMCs.

AlMMC samples with known flaws were purchased from the 3M Corporation. The nature of the flaw in each sample was not well-characterized by 3M Corporation, and the two NDE techniques chosen for this study were challenged to locate and possibly identify the nature of the flaws. It was found through a combination of both NDE and destructive tests that the flaws ranged from quite severe (lack of metal matrix infusion into the fibers over a substantial portion of the specimen) to so insignificant that neither approach could detect anything (copper intermetallic). In one case (fiber waviness), the MWM technique detected an aluminum-rich layer near the surface on one side of the sample. In another case (carbon residue), the ultrasonic C-scan indicated the presence of a possible second defect that was not detected upon a subsequent destructive test. A possible explanation of this false positive is given later in this section.

The goal of the work presented here was to be able to detect flaws that would impact upon the performance of AlMMCs as used in U.S. Army applications. The most severe flaw was lack of infusion (sample 112202-1-2). Both approaches produced scans that imaged the area of lack of infusion, although to somewhat different degrees. The two cracks produced by the carbon residue were clearly indicated in the ultrasonic scan. However, in this particular case the scan produced with the MWM equipment was open to some interpretation. More experience is required to interpret these scans and ensure that variations in material properties are not affecting the conductivity of the sample and possibly masking or altering the response of the signal near the defect.

While cracks, delaminations, and lack of infusion represent gross flaws in AlMMCs, there is another type of material property that is just as important to the mechanical properties of the material. This is fiber volume fraction or fiber content. Xi et al. (2003) have shown that low compressive strength of AlMMC cylinders was attributable to low fiber volume content. That is, fiber volume content is a first-order factor in the mechanical properties of AlMMCs. A low value of fiber volume fraction over an entire sample is generally not considered to be in the same category as a localized defect and thus is hard to characterize as a flaw in that sense. Nevertheless, low fiber volume will be considered a gross flaw for the purposes of this report.

Because fiber volume fraction is such an important material property, an effort was made to relate the sound velocity in the material to the fiber volume fraction. A simple rule of mixtures was used to generate an equation relating the sonic velocity to the fiber volume fraction. Also, it was found that as the fiber volume increases, the return-signal attenuation increases. This is probably due to a higher density of individual scattering bodies (fibers) that decrease the signal strength. Ultrasonic attenuation through pure aluminum is quite low in comparison to that of an AlMMC with 60% fiber volume fraction.

Measurement of sonic velocity also has the advantage that it is an absolute, rather than relative, value. Thus, the fiber volume fraction at specific locations can be determined with ultrasonics. A matrix-rich area (an area of possible weakness) at a critical design point can therefore be detected. (This assumes a suitable part geometry that is conducive to a sonic velocity measurement.) Minimum values of fiber volume content could be specified and parts rejected if they did not meet the criterion.

The fact that the C-scan generated by the Ultrapac equipment is a relative measurement led to misinterpretation of some of the scans done at the beginning of the program. It is clear that gross defects such as cracks or delaminations will lead to high signal attenuation that is represented by a white area in the scan. However, as it was shown in section 6, signal gain can produce the same effect if there are some variations in the fiber volume fraction. In this particular case, a white area (high attenuation) on the scan indicates an area of high fiber volume content. (The possibility of a gross defect in this location was eliminated by microscopic investigation.) It is

not surprising, then, that the mechanical strength in these areas of the University of Delaware samples was higher than that found in areas where attenuation was lower.

Also, it should be noted that thick AlMMC samples with moderate-to-high fiber volume fractions will also produce highly attenuated echo patterns. In this case, a small local increase in fiber volume fraction can produce a white area on a scan. The apparent defect in sample 121202-3-2 (about four times the thickness of the other samples) might be attributed to this effect because no gross defect was found when the sample was sectioned in the area of the apparent flaw indication.

The question is then how to distinguish between high attenuation caused by a crack or delamination and high attenuation caused by a localized increase in fiber volume content. The distinction can be made in some cases where the attenuation is so high that there is little or no reflected signal, indicating that an internal flaw is scattering all the acoustic energy. A highly attenuated echo pattern, on the other hand, would indicate high fiber volume content. Another way is to note the source of the attenuation from the return signal. If there is a large reflected peak at an unexpected location removing some of the energy from the main signal, the attenuation is likely due to a crack or other internal reflecting surface. Note that the ultrasonic approach was unable to detect a matrix-rich layer in sample 121202-3-2 because this nonuniformity was distributed evenly over the entire sample. The nonuniformity was detected by the MWM equipment. This suggests that fiber volume content, a major consideration in material strength, can be determined from a combination of ultrasonics and MWM techniques. That is, a low signal attenuation correlated with a low sonic velocity will indicate low fiber volume content. Matrix-rich layers, which are difficult to detect with ultrasonics, can be revealed with the MWM approach. (Pathological cases where there is a combination of gross cracking and matrix-rich zones would mask the determination of a low fiber volume content. However, the approach would still yield a determination of a material defect.)

While it would be desirable to develop NDE techniques that can be used on an assembly line, it may be that the problem of flaw detection and identification is so complex that an automated process is not possible. As was pointed out in the summary of the literature survey, interpretation of NDE results is best done by a skilled and experienced NDE equipment operator.

Neither ultrasonics nor the MWM approach could unequivocally determine the location or degree of fiber waviness. However, the work of Xi et al. (2003) indicates that fiber waviness may not affect the mechanical properties of an AlMMC material as much as it does in polymer matrix composite systems. This result is quite different from that found for polymer composites. While it is preferable not to have fiber waviness, AlMMCs may be tolerant of such a defect. At some point, fiber waviness will become so great that it does cause loss of material strength. Rather than expend efforts in determining this point, it is clearly more desirable to reduce fiber waviness as much as possible.

8. Summary

The following points summarize this work:

1. A review of the literature indicated that ultrasonic C-scans would be the best way to nondestructively evaluate AlMMCs. In addition, MWM technology was also selected to determine what its potential is for the nondestructive evaluation of AlMMCs.
2. Both ultrasonics and MWM are capable of detecting gross delaminations, cracks, or lack of infusion.
3. A relation was developed between the sonic velocity and fiber volume content. The fiber volume content is considered to be a parameter that is critical to the material strength of AlMMCs.
4. Care has to be taken in interpreting the ultrasonic C-scans. High signal attenuation could be due to the presence of gross flaws or a combination of sample thickness and high fiber volume content. Several suggestions were made to avoid a false positive C-scan reading.
5. Sonic velocity measurements along with MWM measurements were identified as being able to determine in an unequivocal manner low fiber volume content.
6. Neither ultrasonics nor MWM measurements could detect with certainty the existence of fiber waviness. However, a simple observation of the surface of the part generally indicated fiber waviness, especially in AlMMC cylinders that were examined. At this point, a small amount of fiber waviness is not considered to be critical to the material strength of AlMMCs.

9. References

Bar-Cohen, Y. NDE of Fiber-Reinforced Composite Materials – A Review. *Materials Evaluation* **March 1986**, *44*, 446–454.

Bender, J. M.; Dooley, R. C.; Hoppel, C. P. R.; Drysdale, W. H. *Aluminum MMC Projectile Body for Smart Cargo Munitions*; ARL technical report in progress.

Bogetti, T. U.S. Army Research Laboratory: Aberdeen Proving Ground, MD, private communication, 15 July 2003.

Bridge, J.; Butler, J.; Kolli, R.; Klawunder, S.; Lenoe, E.; Hoppel, C.; Dooley, R.; Montgomery, J. Thermal Fatigue Comparison Studies of Alumina Fiber-Aluminum Metal Matrix Composites, *Proceedings of the Army Science Conference*, West Point, NY, November 2001.

Buchanan, D. J.; John, R.; Stubbs, D. A.; Benson, D. M.; Karpur, P. Ultrasonic Longitudinal and Surface Wave Methods for *In Situ* Monitoring of Damage in Metal Matrix and Ceramic Matrix Composites, Symposium on Nontraditional Methods of Sensing Stress, Strain, and Damage in Materials and Structures; ASTM STP 1318: G. F. Lucas and D. A. Stubbs, Eds., American Society for Testing and Materials, New York City, NY, 1997; pp 173–186.

Canumalla, S.; Pangborn, R. N.; Conway, J. C., Jr.; Bhagat, R. B.; Tittmann, B. R.; Dynan, S. A.; Green, D. J. Characterization of Cast, Discontinuous Alumina-Silicate Fiber-Reinforced Aluminum Composites, in *Proceedings of the American Society for Composites 7th Technical Conference*, University Park, PA, 13–15 October 1992; pp 389-399.

Canumalla, S.; Gordon, G. A.; Pangborn, R. N. *Young's Modulus of a Short Fiber Reinforced Metal Matrix Composite*, PVP-Vol 27/NDE-Vol. 12, Determining Material Characterization: Residual Stress and Integrity With NDE, American Society of Mechanical Engineers, 1994.

Chen, F. C.; Netzelmann, U.; Disque, M.; Kroning, M. High Resolution Photothermal Imaging of Metal Matrix Composite Interface *Proceedings of the Seventh International Symposium on Nondestructive Characterization of Materials*, Prague, Czech Republic, June 1995; *Materials Science Forum* **1996**, *210–213*, 447–454.

Chien, H.-T.; Sheen, S.-H.; Apostolos, C. R. An Alternative Approach of Acousto-Ultrasonic Technique for Monitoring Material Anisotropy of Fiber-Reinforced Composites, *IEEE Transactions on Ultrasonics, Ferroelectrics, and Frequency Control* **March 1994**, *41*, (2), 209–214.

Chin, E. U.S. Army Research Laboratory, Aberdeen Proving Ground, MD, personal communication, 26 February 2002.

Dunn, M. L.; Ledbetter, H. Ultrasonic Characterization of the Orientation Distribution of Short Fiber Composites, *Proceedings of the 29th International SAMPE Conference*, 9–12 October 1995; pp 150–158.

Fick, M. J. 3M Industrial and Consumer Markets, St. Paul, MN, private communication, January 2003.

Goldfine, N.; Zilberstein, V.; Cargill, J. S.; Schlicker, D.; Shay, I.; Washabaugh, A.; Tsukernik, V.; Grundy, D.; Windoloski, M. MWM-Array Eddy Current Sensors for Detection of Cracks in Regions With Fretting Damage, *ASNT Materials Evaluation* **July 2002**, *60* (7).

Green, W. U.S. Army Research Laboratory, Aberdeen Proving Ground, MD, private communication, 28 February 2002.

Hall, I. University of Delaware, Newark, DE, private communication, 6 June 2003.

Honarvar, F.; Sinclair, A. N. Nondestructive Evaluation of Cylindrical Components by Resonance Acoustic Spectroscopy, *Ultrasonics* **1998**, *36*, 845–854.

Hoppel, C. P. R.; Beatty, J. H.; Montgomery, J. S.; Bender, J. M.; Bogetti, T. A. Metal Matrix Composite Materials for Ordnance Applications. *Proceedings of the 22nd Army Science Conference*, Baltimore, MD, 11–13 December 2000.

Hoppel, C. P. R.; Drysdale, W. H.; Bogetti, T. A.; Yiournas, A. Structural Design and Optimization of Cargo Carrying Projectiles, *Proceedings of the 5th Joint Classified Bombs/Warheads and Ballistics Symposium*, Colorado Springs, CO, 18–20 June 2002.

Hoppel, C. U.S. Army Research Laboratory, Aberdeen Proving Ground, MD, private communication, December 2002.

Hsu, D. K.; Liaw, P. K.; Baaklini, G. Y. Comparison of NDE Results and Correlation With Microstructural Characteristics of NiFeAl/Wf. *Presented at the International Gas Turbine and Aeroengine Congress and Exposition*, the Hague, Netherlands, 13–16 June 1994; proceedings published by the American Society for Mechanical Engineers, New York, NY.

Johnson, W. S. Screening of Metal Matrix Composites Using Ultrasonic C-Scans, *Journal of Composite Technology and Research, JCTRER* **1989**, *11* (1), 31–34.

Krishnamurthy, S.; Matikas, T. E.; Karpur, P.; Miracle, D. B. Ultrasonic Evaluation of the Processing of Fiber-Reinforced Metal-Matrix Composites, *Composites Science and Technology* **1995**, *54*, 161–168.

Kupperman, D. S.; Majumdar, S.; Singh, J. P. Neutron Diffraction NDE for Advanced Composites, *Transactions of the ASME* **April 1990**, *112*, 198–201.

Lee, J.-H.; Park, Y.-C. Nondestructive Characterization of Metal Matrix Composite by Ultrasonic Measurement, *Composites Engineering* **1995**, *5* (12), 1423–1431.

Matikas, T. E.; Karpur, P. Ultrasonic Reflectivity Technique for the Characterization of Fiber-Matrix Interface in Metal Matrix Composites, *J. Appl. Phys*. **July 1993**, *74*, (1).

Matikas, T. E.; Karpur, P.; Krishnamurthy, S.; Dutton, R. E. A Nondestructive Approach to Correlate the Interfacial Defects Induced During Processing of MMCs and CMCs With the Consolidation Parameters, *Applied Composite Materials* **1995**, *2*, 293–311.

Ostman, E.; Persson, S. Application of X-Ray Tomography in Non-Destructive Testing of Fibre Reinforced Plastics, *Materials and Design* **May/June 1988**, *9* (3), 142–147.

Pipes, R. B. and the Committee on Nondestructive Evaluation of Metal Matrix Composites. Nondestructive Evaluation of Metal Matrix Composites, National Materials Advisory Board Report 413, July 1983.

Schramm, S. W.; Daniel, I. M. Nondestructive Evaluation of Metal Matrix Composites, IIT Research Institute Chicago, IL, under contract to U.S. Army Materials and Mechanics Research Center (Contract No. DAAG46-80-C-0070); AMMRC Technical Report TR-82-35, 1982.

Schwer, L.; Reddy, J. N.; Mal, A. Enhancing Analysis Techniques for Composite Materials, in Proceedings of the Annual Winter Meeting of the American Society of Mechanical Engineers, Atlanta, GA, 1–6 December 1991; NDE-Vol. 10, *Enhancing Analysis Techniques for Composite Materials*, ASME 1991, pp 43–57.

Thompson, R. B.; Thompson, D. O.; Holger, D. K.; Hsu, D. K.; Hughes, M. S.; Papadakis, E. P.; Tsai, Y.-M.; Zachary, L. W. Ultrasonic NDE of Thick Composites, presented at the Winter Annual Meeting of ASME, Atlantic, GA, 1–6 December 1991; NDE Vol. 10, *Enhancing Analysis Techniques for Composite Materials*, 1991, pp 43–57.

Tsangarakis, T.; Gruber, J. J.; Nunes, J. Non-Destructive Evaluation of Fatigue Damage in Alumina Fiber Reinforced Aluminum, *Journal of Composite Materials* **May 1985**, *19*, 250–269.

Wu, T.-T.; Ho, Z.-H. Anisotropic Wave Propagation and Its Applications to NDE of Composite Materials, *Experimental Mechanics* **December 1990**, *30* (4), 313–318.

Xi, Z.; Bogetti, T. A.; Yiournas, A.; Hall, I. W.; Hoppel, C. P. H.; Drysdale, W.; Dooley, R.; Gillespie, J. W., Jr. Analysis, Design and Testing of Metal Matrix Composite Cylinders under Uniaxial Compression, *Proceedings of the American Society for Composites 18th Technical Conference*, Gainesville, FL, October 2003.

Yancey, R. N.; Baaklini, G. Y. Computed Tomography Evaluation of Metal Matrix Composites for Aeropropulsion Engine Applications, *Journal of Engineering for Gas Turbines and Power* **July 1994**, *116*, 635–639.

NO. OF COPIES	ORGANIZATION
1 (PDF Only)	DEFENSE TECHNICAL INFORMATION CENTER DTIC OCA 8725 JOHN J KINGMAN RD STE 0944 FT BELVOIR VA 22060-6218
1	COMMANDING GENERAL US ARMY MATERIEL CMD AMCRDA TF 5001 EISENHOWER AVE ALEXANDRIA VA 22333-0001
1	INST FOR ADVNCD TCHNLGY THE UNIV OF TEXAS AT AUSTIN 3925 W BRAKER LN STE 400 AUSTIN TX 78759-5316
1	US MILITARY ACADEMY MATH SCI CTR EXCELLENCE MADN MATH THAYER HALL WEST POINT NY 10996-1786
1	DIRECTOR US ARMY RESEARCH LAB AMSRD ARL D DR D SMITH 2800 POWDER MILL RD ADELPHI MD 20783-1197
1	DIRECTOR US ARMY RESEARCH LAB AMSRD ARL CS IS R 2800 POWDER MILL RD ADELPHI MD 20783-1197
3	DIRECTOR US ARMY RESEARCH LAB AMSRD ARL CI OK TL 2800 POWDER MILL RD ADELPHI MD 20783-1197
3	DIRECTOR US ARMY RESEARCH LAB AMSRD ARL CS IS T 2800 POWDER MILL RD ADELPHI MD 20783-1197

NO. OF COPIES	ORGANIZATION
	ABERDEEN PROVING GROUND
2	DIR USARL AMSRD ARL CI LP (BLDG 305) AMSRD ARL CI OK TP (BLDG 4600)

NO. OF COPIES	ORGANIZATION
1	US ARMY ARDEC AMSTA AR WEM BLDG 1 M HAGN PICATINNY ARSENAL NJ 07806
1	TOUCHSTONE RESEARCH LAB B GORDON THE MILLENIUM CENTRE TRIADELPHIA WV 26059
1	3M INDUSTRIAL MARKETS 3M CENTER BUILDING 0207-01-SC-12 M FICK ST PAUL MN 55144
2	JENTEK SENSORS N GOLDFINE R MURNER 110-1 CLEMATIS AVE WALTHAM MA 02453-7013
1	SOLIDICA D WHITE 3941 RESEARCH PARK DR. STE C ANN ARBOR MI 48108
1	TRITON SYSTEMS J BURNETT 200 TURNPIKE ROAD CHELMSFORD MA 01824
1	DARPA DSO L CHRISTODOULOU 3701 NORTH FAIRFAX DRIVE ARLINGTON VA 22203-1714
1	AIR FORCE RESEARCH LAB MATERIALS MFG DIRCTRT P MARTIN 2230 TENTH STREET BLDG 655 WRIGHT PATTERSON AFB OH 45433
1	BENET LABORATORIES AMSTA AR CCB T M AUDINO WATERVLIET ARSENAL WATERVLIET NY 12189-4050

NO. OF COPIES	ORGANIZATION
	ABERDEEN PROVING GROUND
30	DIR USARL AMSRD ARL WM B BURNS WM AMSRD ARL WM M B FINK AMSRD ARL WM MB T BOGETTI L BURTON R DOOLEY B DRYSDALE C HOPPEL A YIOURNAS AMSRD ARL WM MC J ADAMS E CHIN G GILDE AMSRD ARL WM MD V CHAMPAGNE W DE ROSSET (10 CPS) R DOWDING W ROY K TACKITT S WALSH R WOODMAN AMSRD ARL WM TC R COATES L MAGNESS AMSRD ARL VT M G FARLEY